New Directions in Seismic Hazard Assessment through Focused Earth Observation in the Marmara Supersite

Grant Agreement Number: 308417
co-funded by the European Commission within the Seventh Framework Programme
THEME [ENV.2012.6.4-2]
[Long-term monitoring experiment in geologically active regions of Europe prone to natural hazards: the Supersite concept]

D8.2

Report On High Resolution Micro Earthquake Characterization

Project Start Date	1 November 2012
Project Duration	36 months
Project Coordinator /Organization	Nurcan Meral Özel / KOERI
Work Package Number	8
Deliverable Name/ Number	Report On High Resolution Micro Earthquake Characterisation/D8.2
Due Date Of Deliverable	31 October 2013
Actual Submission Date	13 November 2013
Organization/Author (s)	IFREMER /Louis GELI KOERI/ Cemil GÜRBÜZ

Dissemination Level		
PU	Public	
PP	Restricted to other programme participants (including the Commission)	
RE	Restricted to a group specified by the consortium (including the Commission)	
CO	Confidential, only for members of the consortium (including the Commission)	

Contents

Summary

A study was carried out within Work Package 8 (WP8) of MARSITE in order to improve the characterization of the near-fault micro-seismicity within the Sea of Marmara. Velocity models were thus developed by KOERI and Ifremer respectively, following two different approaches:

- *KOERI developed a 3D velocity model for the whole Marmara Region (within latitudes 39.5°N - 42.5°N and longitudes 26.0°E - 30.5°E), including land and seabottom stations, with grid spacing of 9 km x 9 km x 3 km.*

- *Ifremer developed an opposite, but complementary approach, strictly based on seabottom stations, for the Western Sea of Marmara (40°43'N - 40°54'N – 27°30'E – 28°15'E). A high resolution velocity model with a 750 m x 750 m x 400 m grid spacing was built, using multibeam bathymetry and wide-angle seismic data, in order to account for the velocity contrast at the water/sediment interface and the slow seismic velocities within the sediment infill in the main Marmara Trough.*

The velocity model developed by KOERI for the whole Marmara region by merging land and sea stations appears to be very useful to improve the quality of earthquake catalogs and the real time monitoring of the regional seismicity.

In contrast, to improve the final-scale location of hypocenters near the submerged fault zone and enhance the search for seismic tremors, specific networks of permanent, cabled sea-bottom seismometers are required. Each network should be consistent per se, and allow the high-resolution characterization of earthquakes below the Sea of Marmara. In addition, it is of critical importance to create an high-resolution, 3D velocity model, in order to take into account for the velocity contrast at the water/sediment interface and the slow seismic velocities within the sediment infill in the main Marmara Trough.

I. Introduction

The general objective of WP8 is to implement an integrated approach based on multi-parameter seafloor observatories, to continuously monitor the micro-seismicity along with the fluid expulsion activity within the submerged fault zone. The discovery of very characteristic tremors, 44 minutes prior to the Izmit earthquake in 1999 [*Bouchon et al., 2011*], and the finding that gas reservoirs are connected to the Main Marmara fault zone [*Bourry et al., 2009 ; Géli et al., 2008 ; Gasperini et al., 2012*] opens new perspectives that were not imaginable a few years ago: if seismic tremors are found to be associated with clear anomalies in gas emission activity, then we will have more criteria for characterizing and identifying the recorded signals as indicators that the probability of occurrence of an impending earthquake is increasing. WP8 will hence contribute to find robust and multiparametric methods for implementing early warning strategies in the near future.

One specific objective of WP8 is to detect low magnitude earthquakes and improve the characterization of the near-fault micro-seismicity, particularly along the central part of the SoM. To meet this objective, velocity models were developed by KOERI and by Ifremer to improve earthquake location in the Sea of Marmara, following two different approaches:

I.1 KOERI has developed a 3D velocity model for the whole Marmara Region (within latitudes 39.5°N - 42.5°N and longitudes 26.0°E - 30.5°E), including land and seabottom stations, with grid spacing of 9 km x 9 km x 3 km.

I.2 Ifremer has developed an opposite, but complementary approach, strictly based on seabottom stations, for the Western Sea of Marmara (40°43'N - 40°54'N – 27°30'E – 28°15'E). A high resolution velocity model with a 750 m x 750 m x 400 m grid spacing was built, using multibeam bathymetry and wide-angle seismic data, in order to account for the velocity contrast at the water/sediment interface and the slow seismic velocities within the sediment infill in the main Marmara Trough.

These two approaches are reported in the present deliverable D8.2.

II. Velocity model at the scale of the Marmara Region for improving earthquake catalogs

II.1 Data sets

The data consist in first arrival times detected from seismograms generated by earthquakes and by seismic shots. For practical reasons, 2 datasets are considered, as indicated in Table 1:

- The "small dataset" (also called dataset 1) includes travel times from earthquakes that occurred between October 1st, 2009 and December 31st, 2011, below the Sea of Marmara and the near surroundings, e.g. within coordinates 26.5°E - 30°E – 40.2°N – 41.2°N. A total of 1320 earthquakes occurred in the area during this period, but only 620 events were considered of acceptable quality and used for tomographic purposes. The travel times were recorded by 87 permanent, land stations and by 5 permanent, cabled, seabottom stations, operated by KOERI.
- The "large dataset" (also called dataset 2) includes travel times from earthquakes that occurred between October 1st, 2009 and December 31st, 2012, over a large area encompassing part of the Black Sea, the Eastern Marmara and Thrace Regions (26°E-30.5°E – 39.5°N-42.5°N), so as to increase the number of earthquakes and improve the resolution on land. The travel times were recorded by 98 permanent, land stations and by 5 permanent, cabled, seabottom stations, operated by KOERI.
- In addition, both datasets also include :
  - Travel times recorded during 2 limited time windows (from October 1st, 2009 to March 15th, 2010, and from April 15th, 2011 to July 31st, 2011), using non-permanent sea bottom stations from Ifremer.
  - Travel times generated by seismic shots produced by R/V Nadir during the Seismarmara cruise in 2001. The seismic shots were recorded by the land stations that were available in 2001, and by 37 non-permanent, seabottom stations (from Hokkaido University) specifically deployed for the duration of the Seismarmara cruise (see purple dots in Figure II.1).

"LARGE DATASET" or DATASET-2						
	Origin of stations	# of stations	Start recording period	End recording period	# of earthquakes	# of shots
Land stations	KOERI	52	1st Oct. 2009	31st Dec. 2012	-	-
	TUBITAK	41	1st Oct. 2009	31st Dec. 2012	-	-
	TR Project	5	1st Oct. 2009	31st Dec. 2012	-	-
Sea bottom stations	KOERI (OBO)	5	1st Dec 2009	31st Dec. 2012	-	-
	Ifremer-1	12	1st Oct. 2009	15th Mar. 2010	-	-
	Ifremer-2	10	15th April 2011	31st July 2011	-	-
	Seismarmara	37	2001	2001	-	650
				TOTAL=	3700	650

Table 1 : Datasets used in the present study.

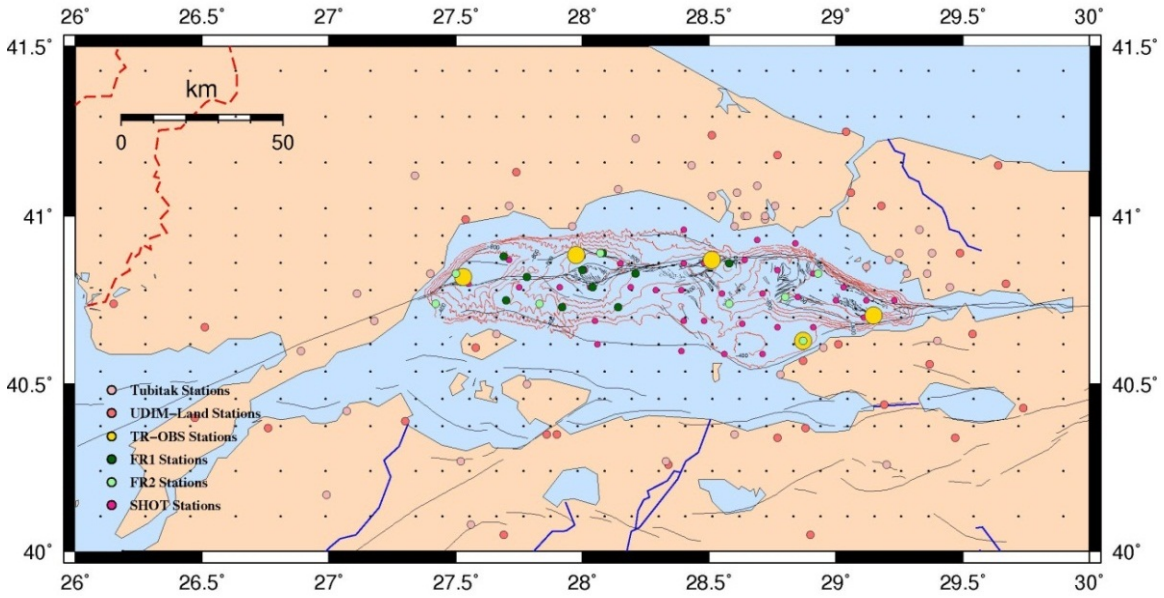

Figure II.1. Station distribution used in the study

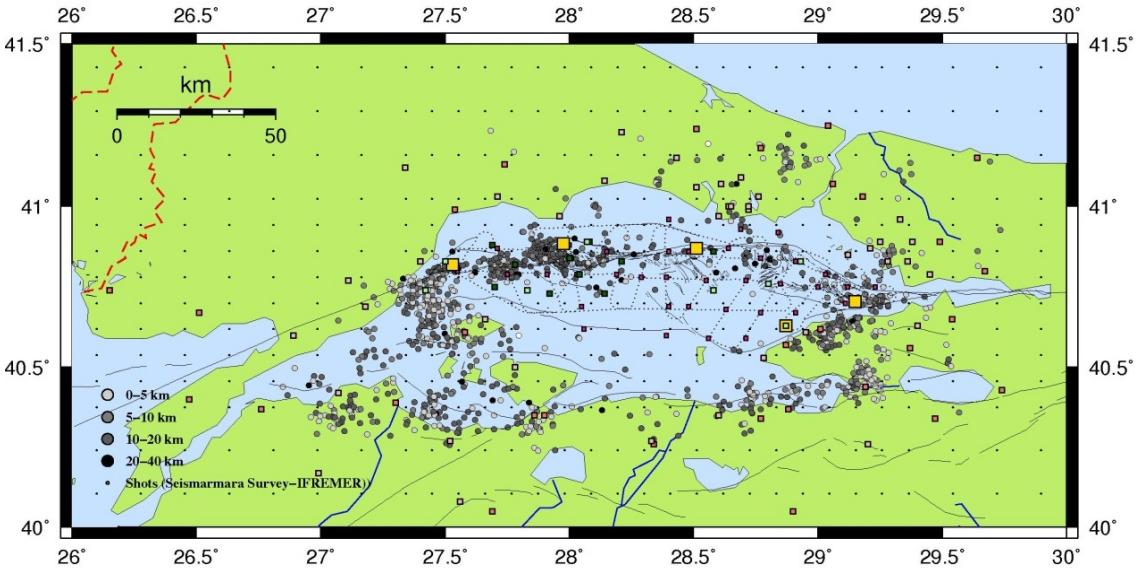

Figure II.2. "Small dataset" used in the present study

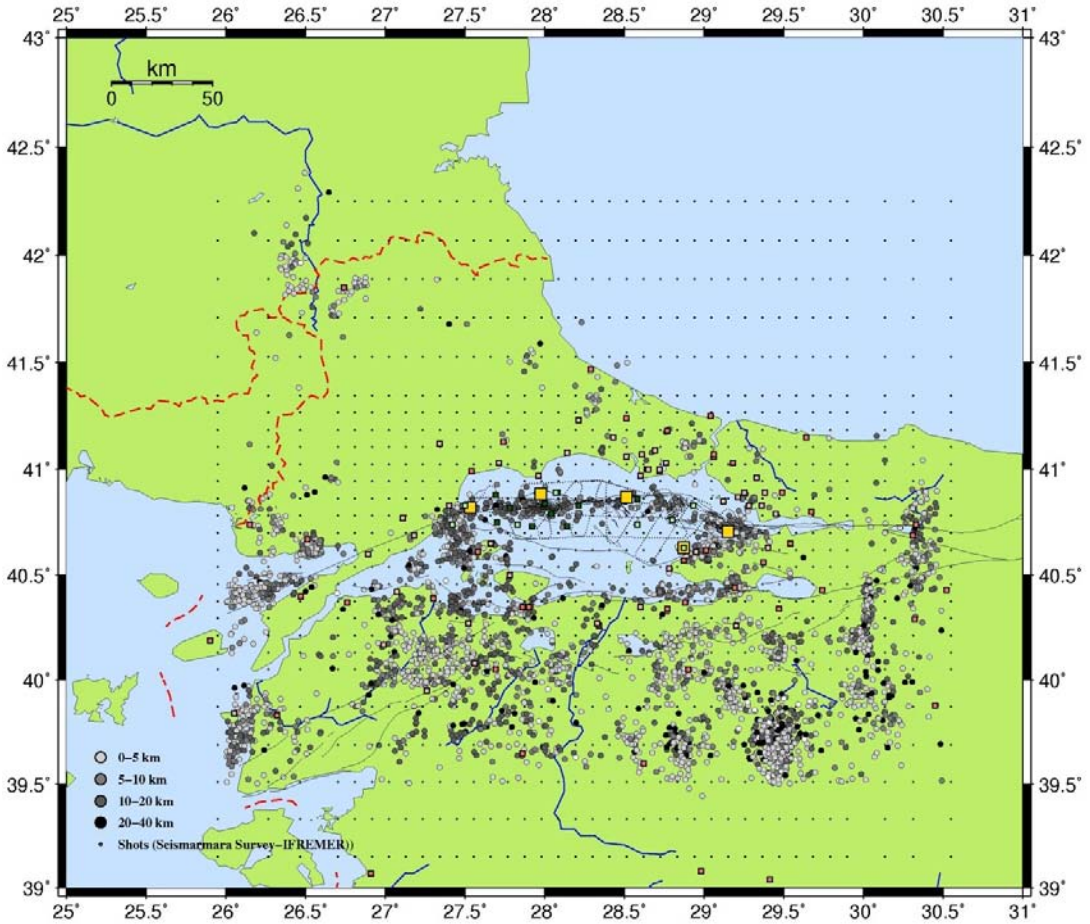

Figure II.3. "Large data set" used in the present study

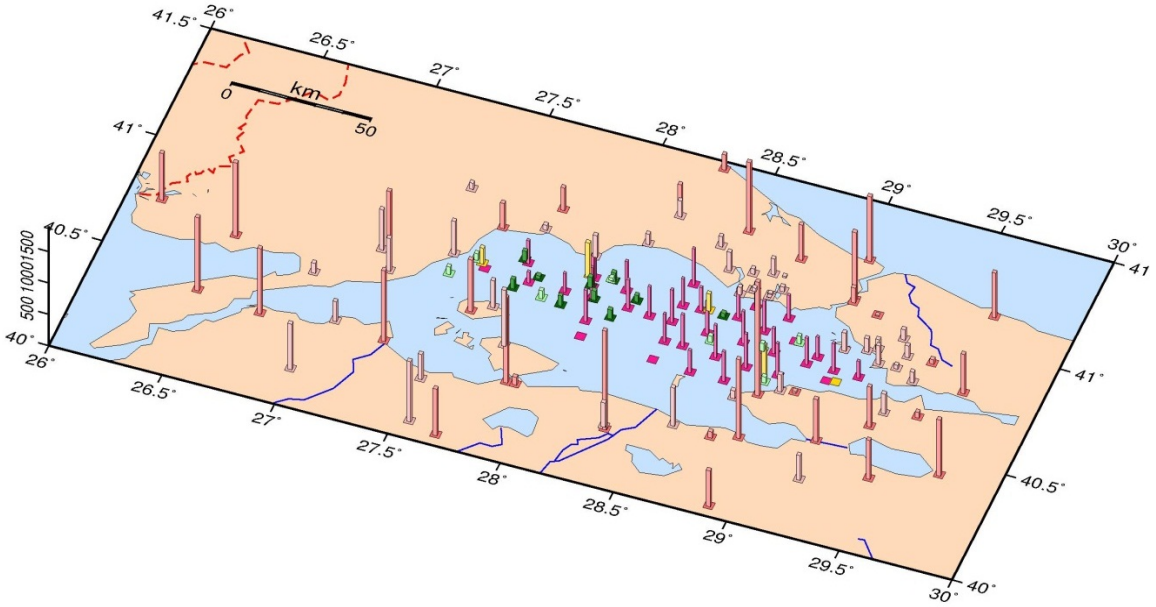

Figure II.4. Number of recordings per station. The number of recordings at stations located north of the Marmara Sea is remarkably less than those located to the south. Also, light green (FR) and dark green stations (FR) have less recordings compared to those on land. However, the pink stations which recorded the shots provide a good ray coverage with dense data. The light pink stations of TUBITAK fill the gap around the Marmara Sea but with less data then KOERI stations on land. Light orange stations of KOERI located at the outer boundary of the study area have the largest amount of recordings.

II.2 Derivation of the minimum 1D model

The data from October 1st 2009 until 31st July 2011 consists of 1320 earthquakes. These were located with hypocenter program. A total of 700 earthquakes were eliminated, considering the quality factors such as the gap, latitude error, longitude error and number of stations recorded the earthquakes. The 620 remaining earthquakes were then used for deriving a minimum 1D velocity model and a 3D velocity model. The first time arrival picking and the 1D minimum model deriving steps were made through out SEISAN.

After deriving the 1D minimum model, the second part of land data (from 31st July 2011 to 31st December 2012) was added to the data set in order to improve the resolution within the land area. This second part of the data, which was not included in the 1D minimum model deriving process, consists in 738 well located earthquakes, based on land and OBO stations. In total the tomography process was carried out with 1358 earthquakes and 650 shots.

II.3 First 3D inversion, based on the minimum 1D model as initial model

The 1D-velocity model supposed to represent Marmara Region, was used to develop the 3D P-wave velocity model. However, since the Marmara Region with its deep sub-basins shows high velocity contrast, the 1D model did not yield to the expected 3D velocity model, although both the initial control parameters and the grid space were carefully selected by making several test inversions.

- First the grid space was chosen by making checkerboard tests with the small dataset containing 1300 earthquakes (TR) and 650 shots (FR) and the large dataset with 3700 earthquakes (TR) and 650 shots (FR). Eventually, the selected grid space was 9*9 km.
- The second step was to choose the initial control parameters and to test their effectiveness through several inversions. First, we tried varying maximum allowed P wave velocity perturbations to if the reason for insufficient P-wave velocity distribution under and around the sea area was the iteration number or the maximum allowed P-wave perturbation for each iteration. A 0.25 maximum allowed P-wave velocity perturbation and 9 iterations was eventually chosen for the preliminary inversions.
- The optimum damping value was also selected by classical method and chosen as 90.

The most significant aim of this tomographic inversion was to create a model supposed to represent the area with both land and sea stations. However, the resulting 3D model, derived from 1D minimum model, with the selected initial control parameters, grid space and damping value did not yield a satisfactory model (note that the sea area was solved more precisely than the land area). So we searched a new 1D model within the resulting 3D model.

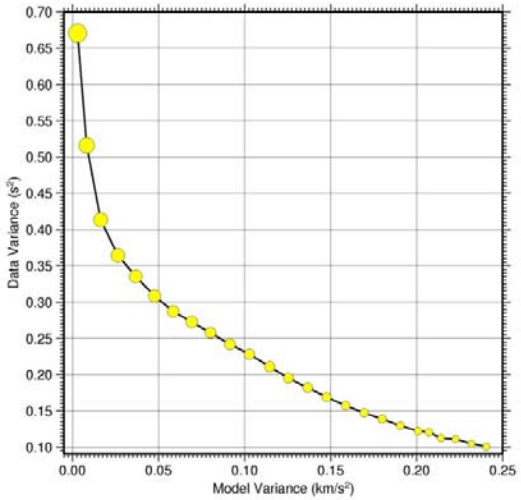

Figure II.5. Data Variance Reduction with damping 0.1 km/s

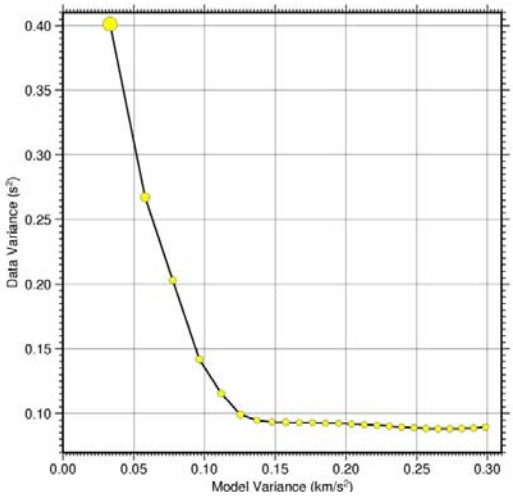

Figure II.6 . Data Variance Reduction with damping 0.25 km/s

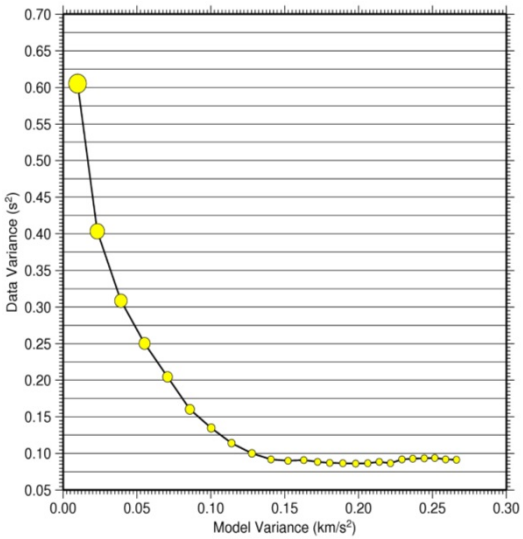

Figure II.7. Data Variance Reduction with damping 0.25 km/s

II.4 Search for a new initial model

A number of 1D models were extracted from the first 3D model from different points representing the Istanbul Zone, the Sakarya Zone, the Thrace Basin, the Çınarcık Basin and the Central Basin. Initial control parameters were decided for each 1D extracted model by making several inversions.

Then, 3D inversions (for each 1D model used as initial 3D model) were made. When the results were compared according to both consistency of velocity model with the geology of the region and RMS improvement of earthquakes, the Istanbul Zone and the Central Basin models were selected to be the best models that would represent the region. However, still the depth of the sedimentary deposits of the sub-basins and the medium under the land around the sea were not sufficient. So, to test, we first created a model which has İstanbul Zone model at all depths but has Central Basin model under the basins until 6 km. the second combined model has the same velocities as in the Central Basin model until 6 km and the rest has the Istanbul Zone model. The aim to create these models here is to understand which part of the 1D model prevents a good inversion on the problematic areas. The first combined model includes low velocities only under the basin. The second combined model has low velocities until 6 km where we expect to see the end of the basin infill [*Becel, 2006*]. After seeing that what makes the resulting model unrealistic at basin rims is that these zones have transitional velocities we decided to add intermediate velocities to these areas which is also suggested by [Bayrakçı, 2009].

The combined initial models showed different velocity distribution in the region. Comparing the results we decided to use the third “combined” model to be the initial model since both the velocities under land and sea are better represented.

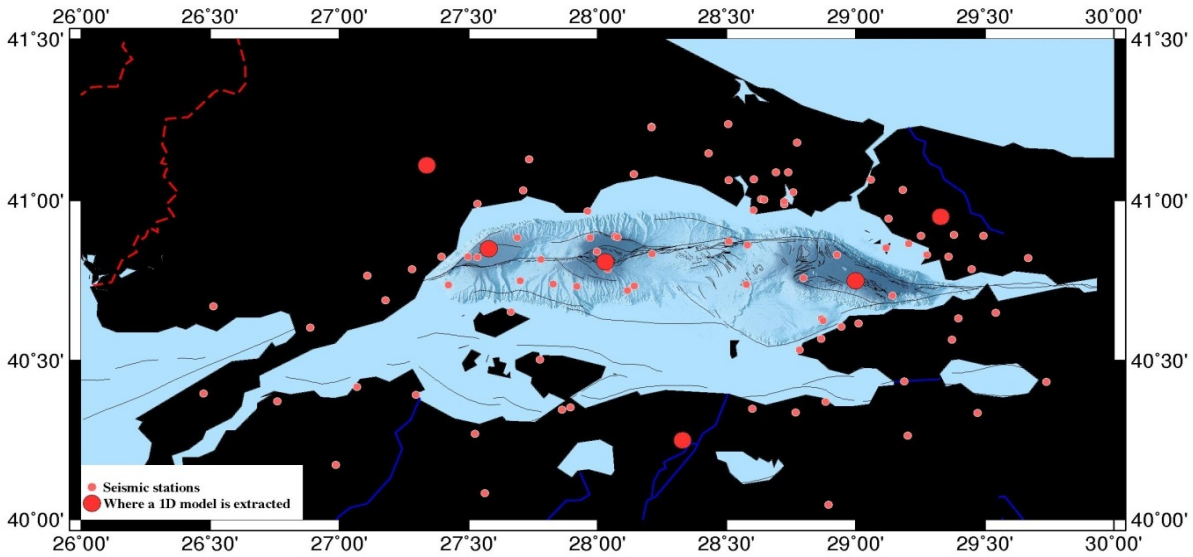

Figure II.8. Points where 1D models were extracted from the resulting 3D model and Station Distribution

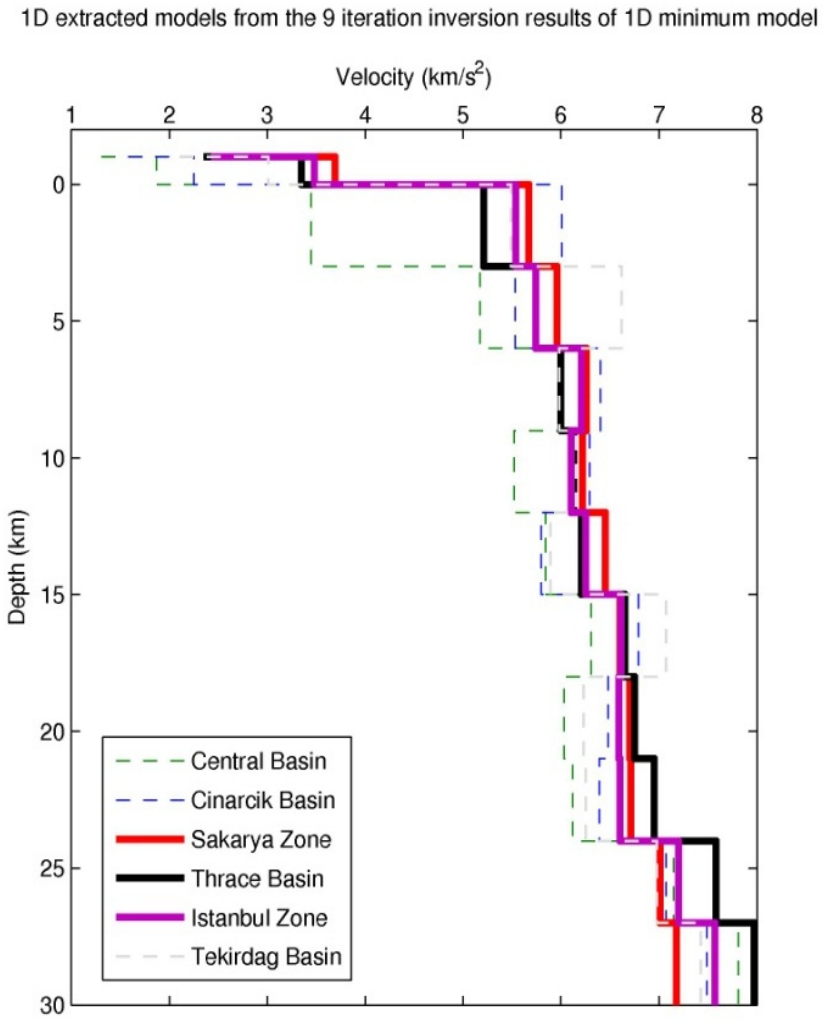

Figure II.9. 1D models extracted from the 3D inverted model

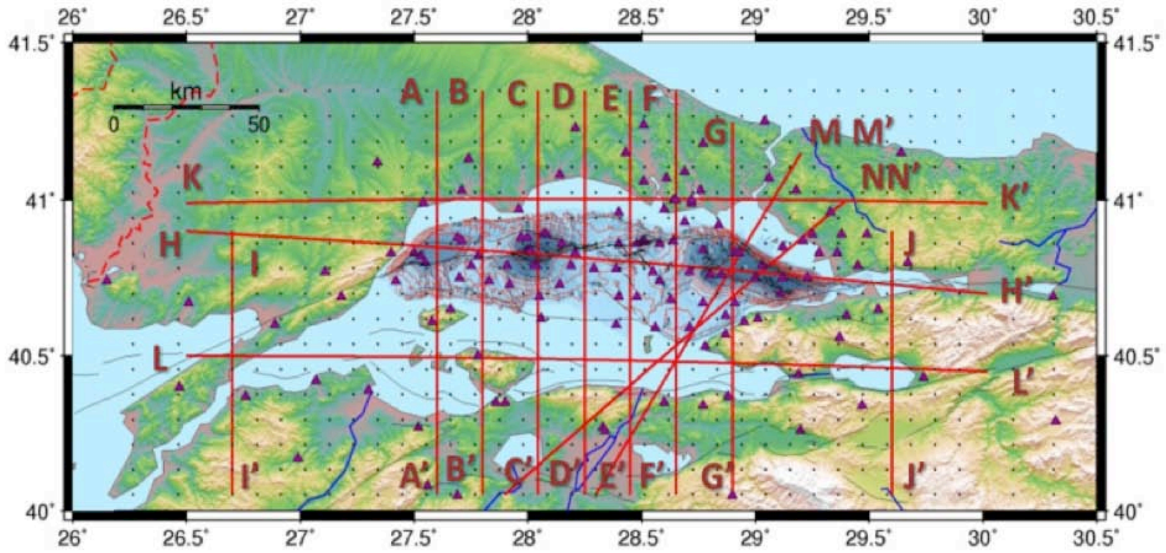

Figure II.10. Cross sections extracted from the resulting 3D models.

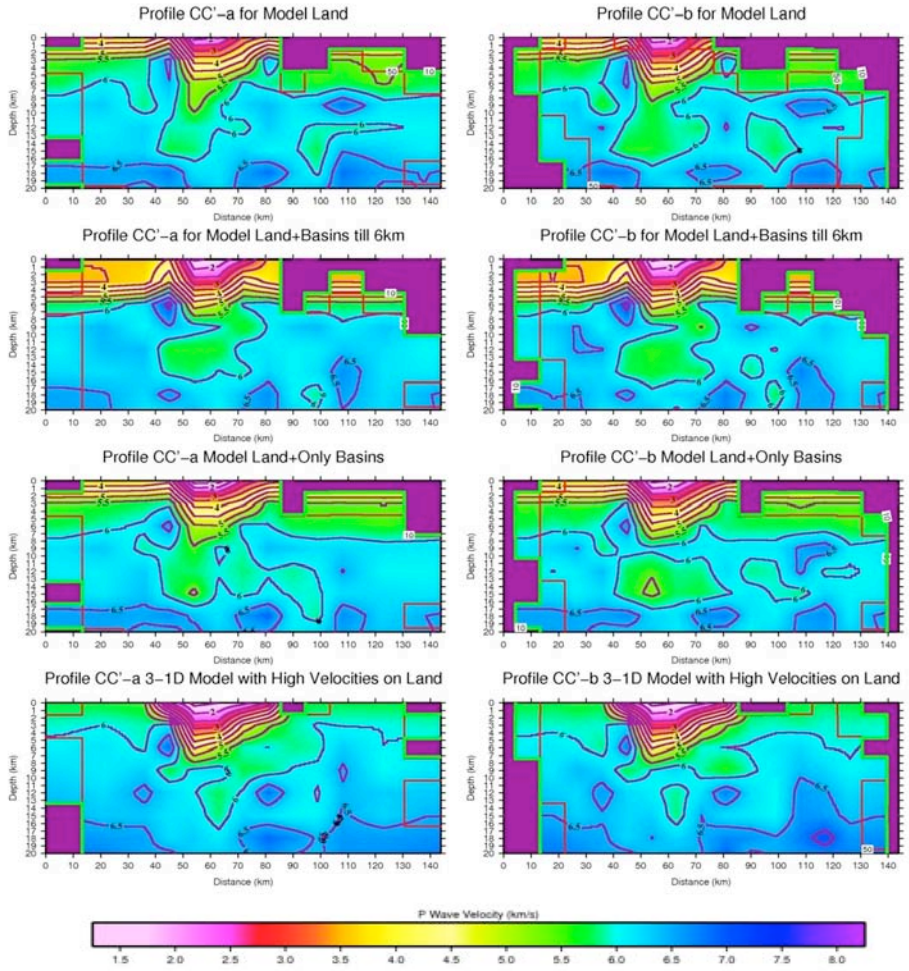

Figure II.11. Cross-Section CC'. Left hand side maps: inversion results of large area dataset. Right inversion results of small area data set.

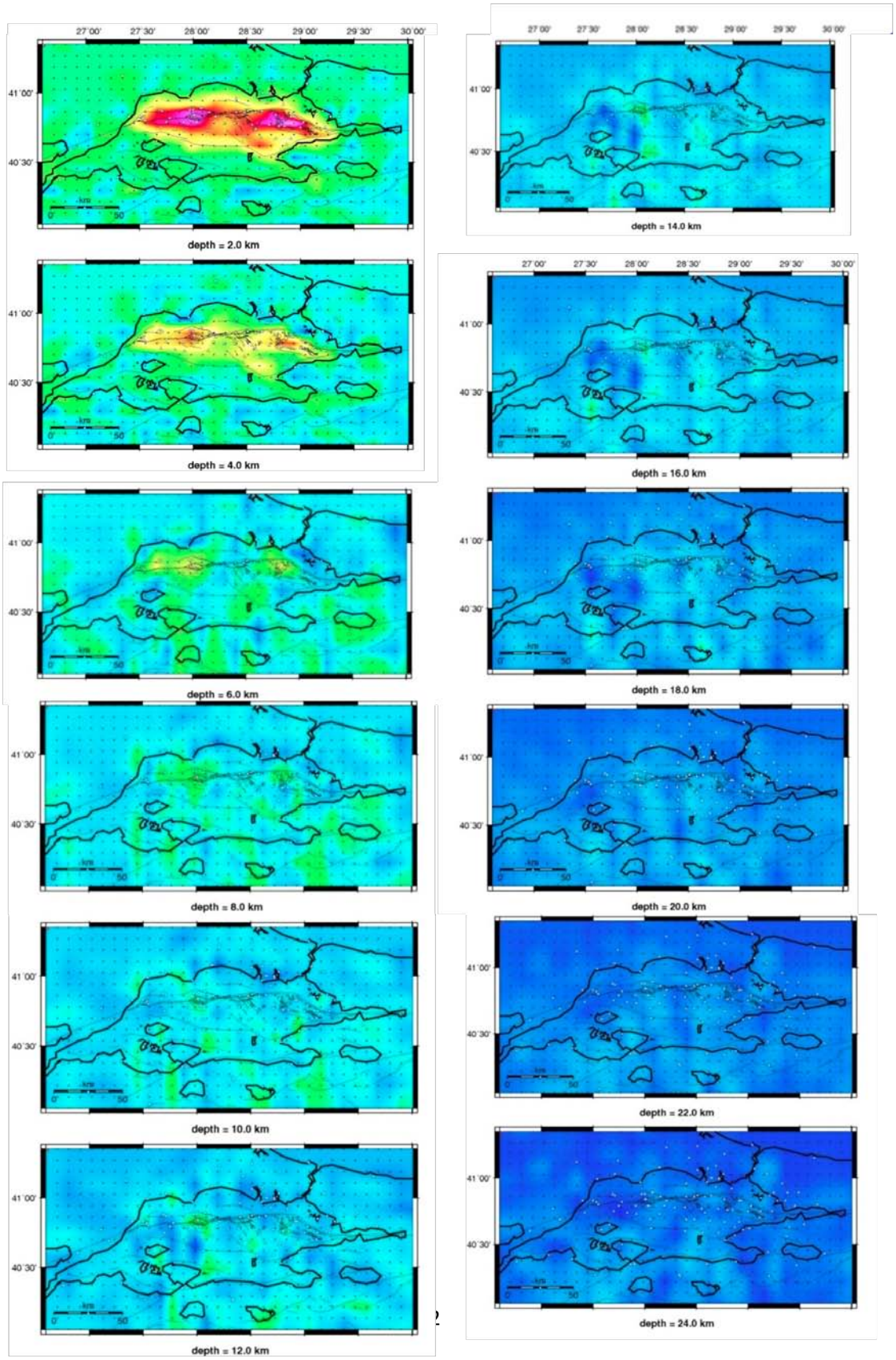

Figure II.12a. Inversion results of the third ("combined") model. Inversion results of large (left) and small (right) area dataset.

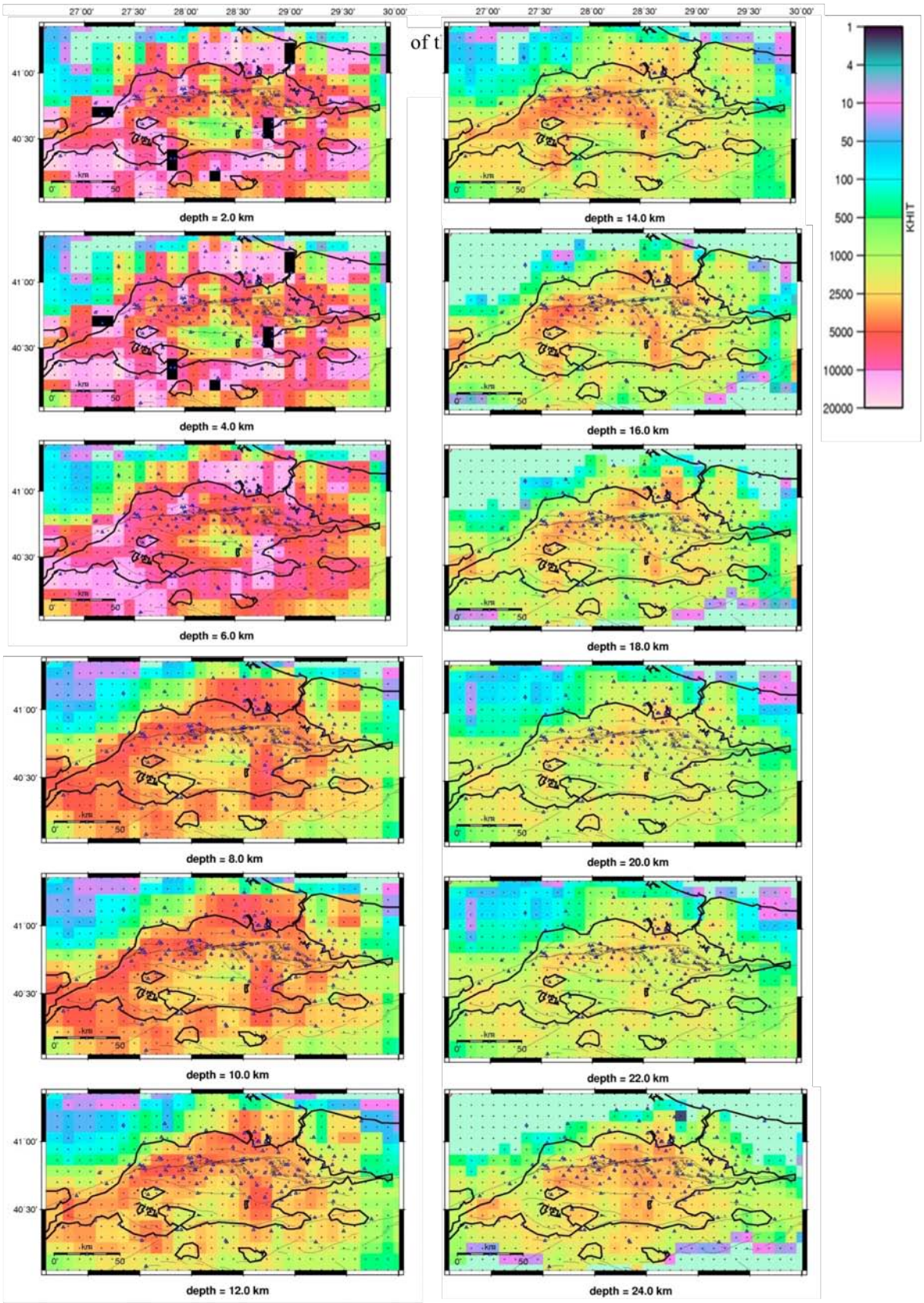

Figure II.12b. Hit count distribution of the third, "combined" model. Inversion results of large (left) and small (right) area dataset.

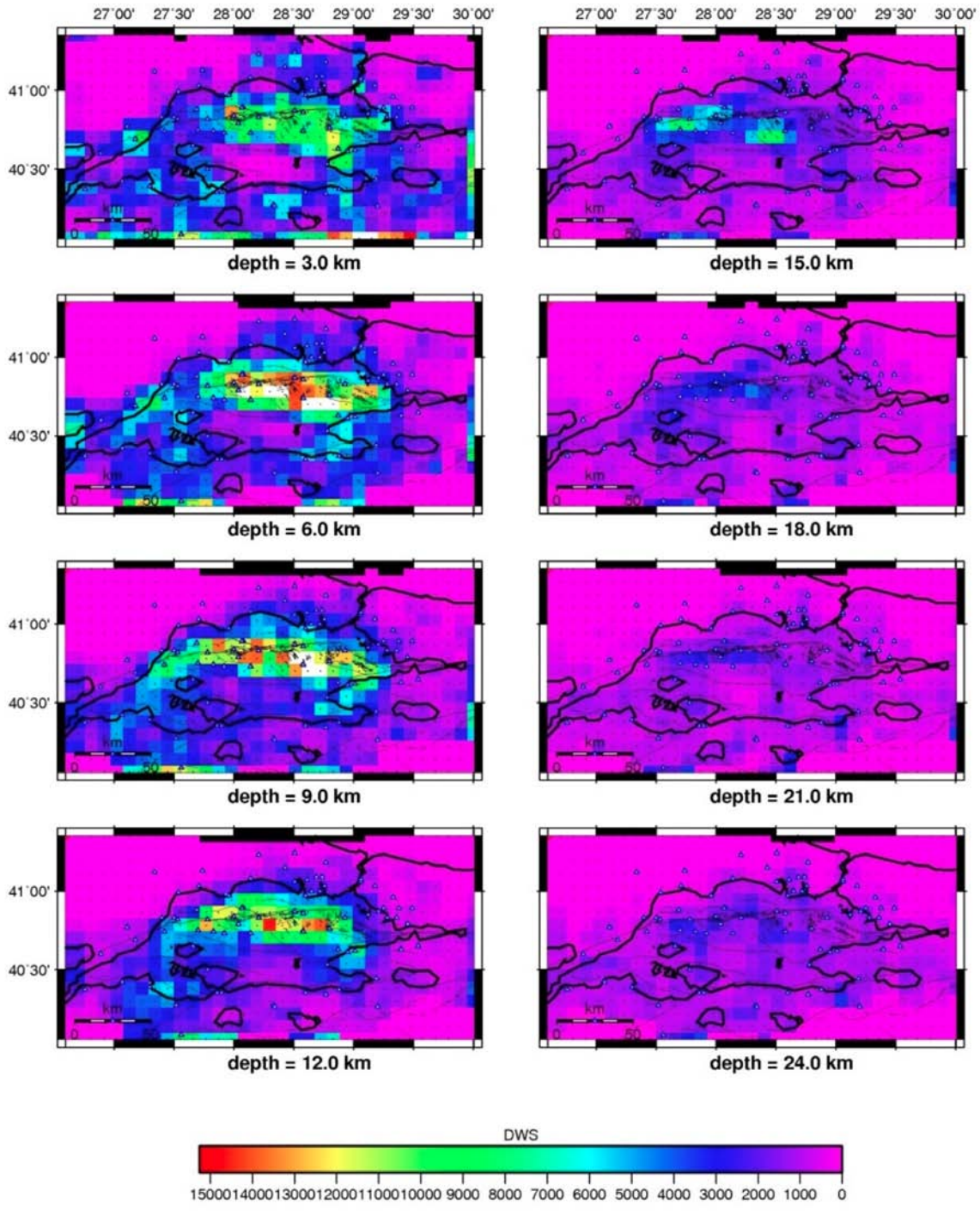

Figure II.13. DWS distribution of the third "combined" model. Inversion results of large (left) and small (right) area dataset.

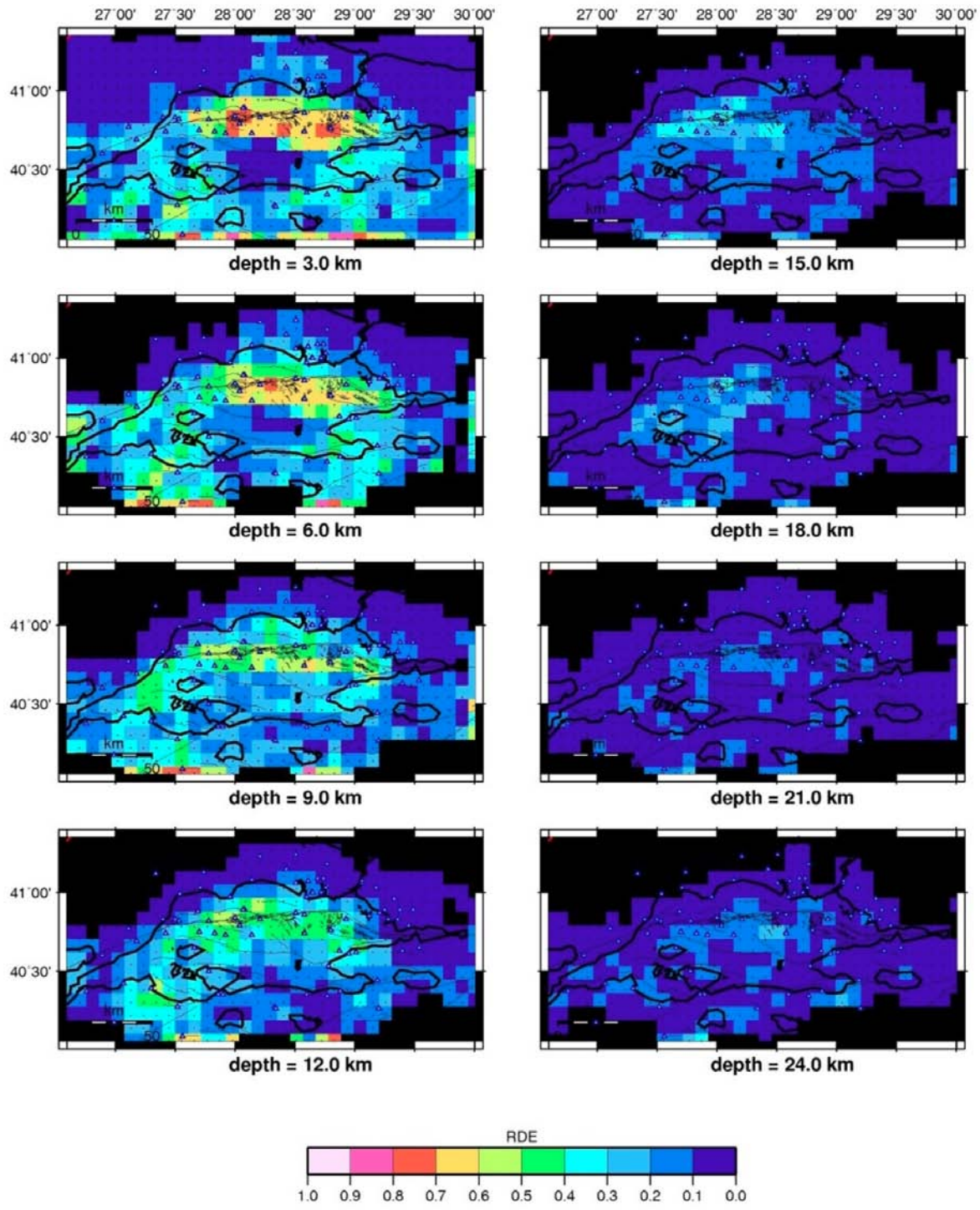

Figure II.14. RDE distribution of the third "combined model". Inversion results of large (left) and small (right) area dataset.

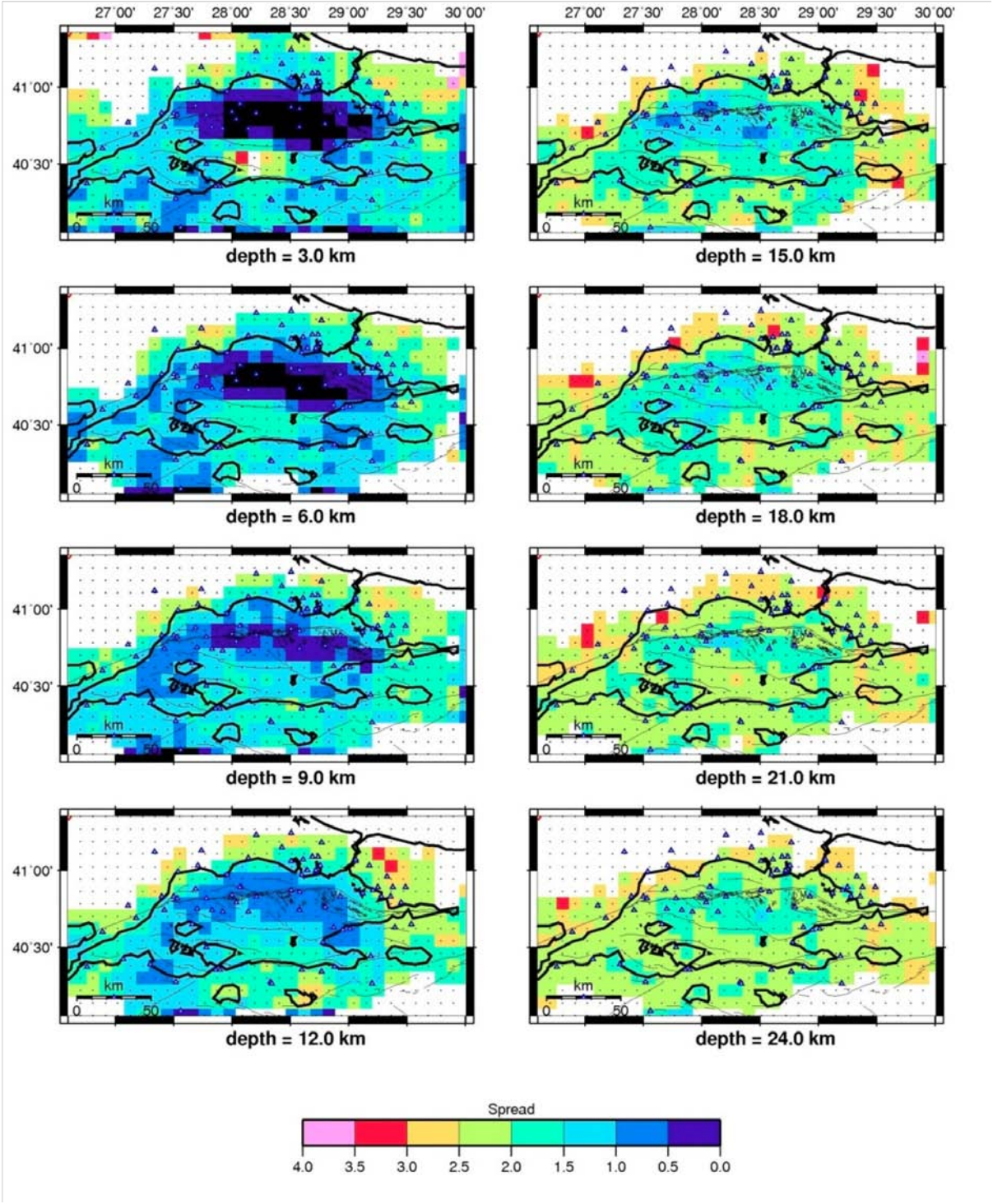

Figure II.15. Spread function distribution of the third "combined" model. Inversion results of large (left) and small (right) area dataset.

II.5 Resolution

The checkerboard test is an application which shows the image distortion in the medium [*Spakman, 1993; Zhao et al., 1992; Benz et al., 1996; Zelt & Barton, 1998; Zelt et al., 2001; Tong et al.,2003*].

The perturbation percentage has a critical effect on the results of the test. If injected anomalies are different from the real ones the results would not be sufficient to understand the real coverage [*Lévèque et al., 1993*].

In order to see how much the study medium covered by the data, realistic high and low velocities have been injected into the 3rd combined model. This time being different from the previous checkerboard tests, we inserted high perturbations only to the nodes along the basins. By making this we aim not to disturb too much the land areas. In the resulting model we observed velocity perturbations nearly −30% in the sea where the land areas showed maximum ±10%. The related nodes perturbed as ±30% and ±10% at 3km and as ±20% and ±10% at 6km. We preferred to decrease the perturbation at 6 km because the resulting model had less than ±30% perturbation. The land areas showed similar variations nearly at all depths so the perturbation has been kept fixed as ±10%. By looking at the real structures both in the sea and the land the checkerboard pattern designed as an 18*18 grid. After adding a Gaussian noise to the results of the synthetic travel times, we made an inversion with the same control parameters as in the real one (damping=95, velocity perturbation=0.25, 6 iterations).

Figures II..16 and Figure II..17 show the checkerboard pattern applied to the data and the synthetic inversion results. We see a very good coverage in the sea at all depths until 24km. The coverage is coarse in the northwest and northeast corners of the study area. Southern Marmara shows a good coverage.

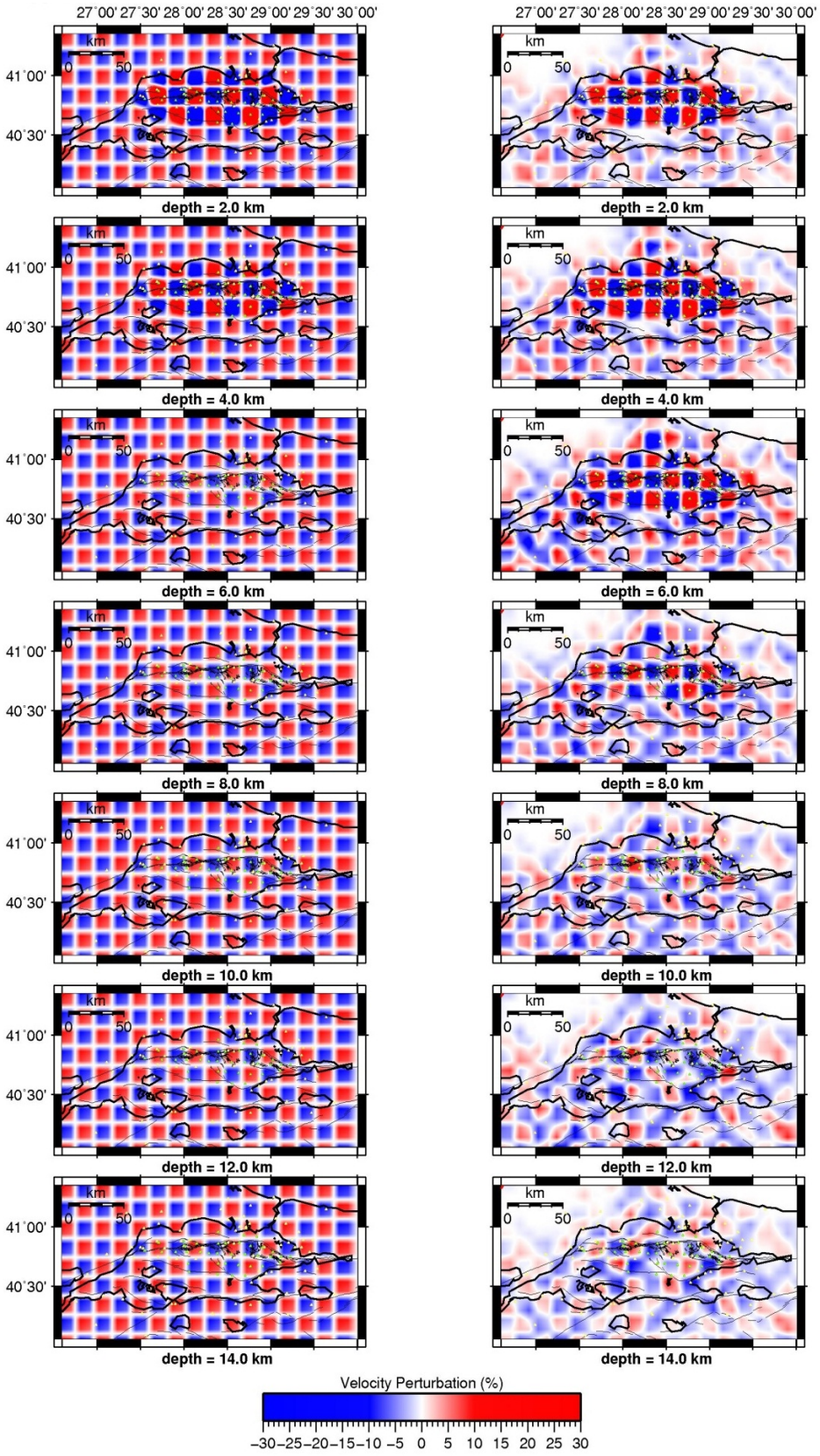

Figure II.16. Checkerboard Test 2km-14 km. Inversion results of large (left) and small (left) area dataset.

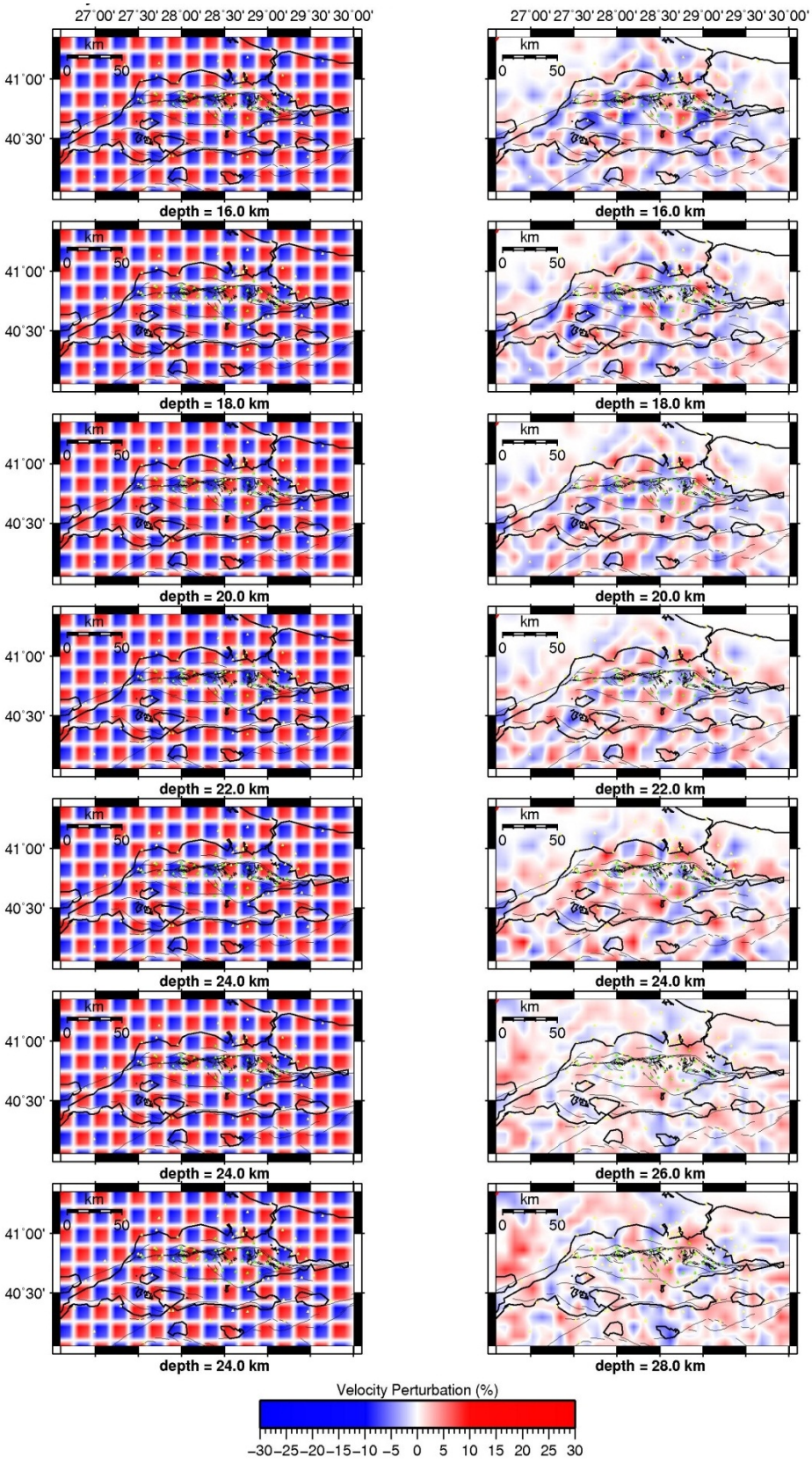

Figure II.17. Checkerboard Test 2km-14 km. Inversion results of large (left) and small (right) area data set.

II. 6 Relocations with the "combined" 3D Model

In this section we want to show the differences between a priori and a posteriori locations before and after the 3D inversion:

- Figure II.18 shows the sequence of aftershocks that followed the earthquake of magnitude 5.2, which occurred on the Western High, on 25th of July 2011, at 17h57 appear more gathered and shallower. The 3D location has a remarkable effect on the depths of the earthquakes.
- Figure II.19 shows the relocation of earthquakes of magnitude > 3 that occurred in Marmara Region. Earthquakes get shallower in the sea, where the 3D model includes low sediment velocity not like the 1D minimum model. There is also a change around the Gemlik Bay because the initial model has been inverted in south more remarkably due to the dense earthquake data.

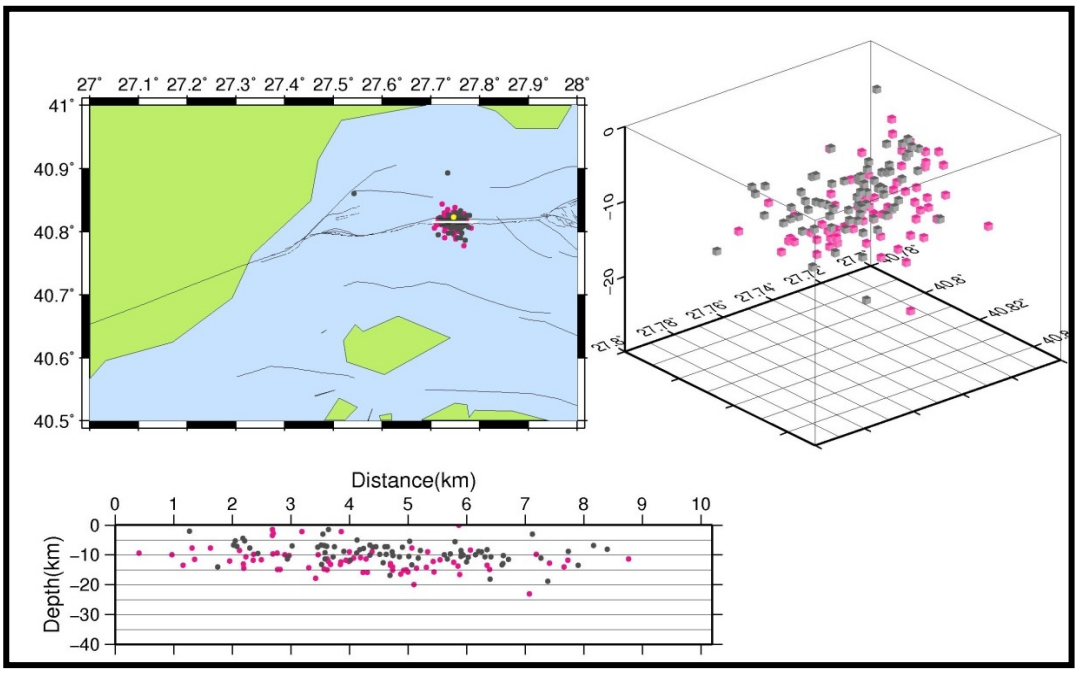

Figure II.18. Relocation of the adftershock seuence that followed the Mw 5.2 earthquake that occured on 25th July 2011, 17:57, on the Western High. Distance is computed along the white line shown on the map. Gray and pink dots show a posteriori and a priori locations, respectively.

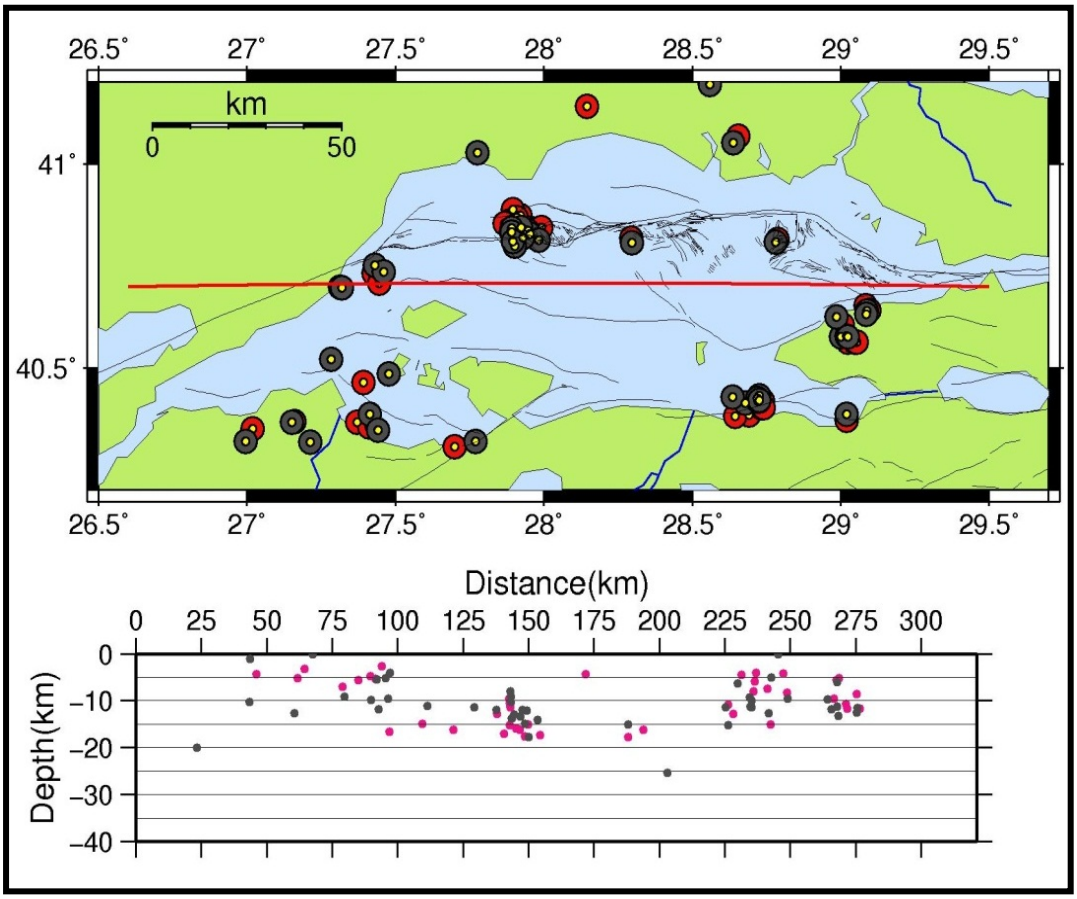

Figure II.19 Relocations of earthquakes of magnitude > 3 in the Marmara Region. Gray and pink dots show a posteriori and a priori locations, respectively.

II.7 Discussion

In the present study we showed the 3D velocity variation in Marmara Region. Thanks to previous studies [*Becel, 2006 ; Becel, 2009 ; Bayrakçı, 2013*], we are able to compare the results with MSC (multi-channel seismic), WARR (wide angle reflection, refraction) and shot tomography studies applied in Marmara Sea. However, these studies do not include velocity information from the land stations. So, we will discuss the inversion results of the land areas with respect to the synthetic test results. The shot tomography study applied in Marmara Sea only gives information of upper crust until 12 km but the WARR and MSC studies revealed both the whole crust and the Moho. In our study we could not interpret the results of the inversion after 24 km because of the low resolution.

The velocities of the pre-kinematic basement and the crystalline basement are defined as 4.5 km/s and 5.7 km/s, respectively [*Bécel, 2006 ; Bécel et al., 2009*]. All the cross sections are consistent with the previous studies; thanks to the shot data from the multi-method survey Seismarmara (2001), we improve the ray coverage in the center of the study. The entire basin area is well resolved according to the RDE, SF and DWS values. Only the northern land area is not well resolved compared to the rest of the study region.

In the previous shot tomography study, the velocity structure at the western edge of the Tekirdağ Basin could not be understood because of the low resolution there. In the result of the 3rd combined model, the RDE, SF, DWS and hit count have better values than the previous study. Thus, we can make interpretation on the results around Tekirdağ Basin due to the DWS >1000, which we rely on until 21 km.

All the basin area shows similar depths of pre-kinematic and crystalline basement with respect to previous studies [*Becel, 2006; Becel et al., 2009; Bayrakçı, 2009]*. Sediments deposits in the sea exhibit very low velocities as 3-3.5 km/s with almost the same depths between 5 and 6 km. The velocity contrast between land and sea becomes negligible below 10 km. The upper crust below 10 km has the average velocity between 6 km/s and 6.3 km/s until Conrad discontinuity. Although we had an idea of the upper limit of the lower crust from the inversion results, we do not observe a clear depth variation of the Conrad. We can still say that under every basin the Conrad contour shallows towards the basin, which is also suggested by [Bécel, 2009].

We do not observe a similarity between Western High and Central High. The pre-kinematic basement under the Western high is located at 5.5 km while it is located at 4 km under the Central Basin. [Bayrakci, 2009], suggested that the Western high most likely results from a sedimentary fold than from a basement rise.

The İmralı and Çınarcık Basins are separated from each other with contrast high velocity zone. The thickness of the sedimentary infill of the İmrali basin is close to the Çınarcık basin and they are separated from each other by the crystalline basement which makes a rise up to 2-3

km. From 12 km to 18 km we observe a high velocity zone compare to its vicinity located north of the Kapıdağ Peninsula in NW-SE direction which can be raleted to the rise of the lower crust here. However, we do not observe high velocity zones as significant as under the Tekirdağ Basin, which might result from the insufficient ray coverage here.

The lower crust velocity information showed similarities under the Central Basin and the Çınarcık Basin. These are surrounded by high velocity zones, which can be accepted as an indicator of normal faulting. Between 8 km and 12 km, the northern edge of the European side of the Marmara Region exibits velocities of 6 to 6.5 km/s.

III. Local velocity models for the North Marmara Trough for the high resolution characterization of earthquakes within the fault zone

III.1 Study area

The study area has been specifically designed for the high-resolution characterization of earthquakes within the fault zone in the Western Sea of Marmara, including the Tekirdag Basin, the Western High and the Central Basin. In order to avoid artifacts related to abrupt topography (sharp slopes, escarpments, canyons, etc), the area only includes the deepest parts of the submarine domain. It is elongated in the direction of the Main Marmara Fault (~60 km from E to W and 20 km from N to S) and located within coordinates 40°43'N - 40°54'N – 27°30'E – 28°15'E.

In 2011, the study area was monitored by 9 non-permanent OBSs from Ifremer, which recorded data during 107 days, from April 15th to July 31st, 2011 (except for OBS2, which unfortunately failed 31 days before the end of the deployment), complementing the permanent monitoring provided by the 2 westernmost stations (KOERI-4 and KOERI-5) of the KOERI's permanent, submarine network (Figure III.1).

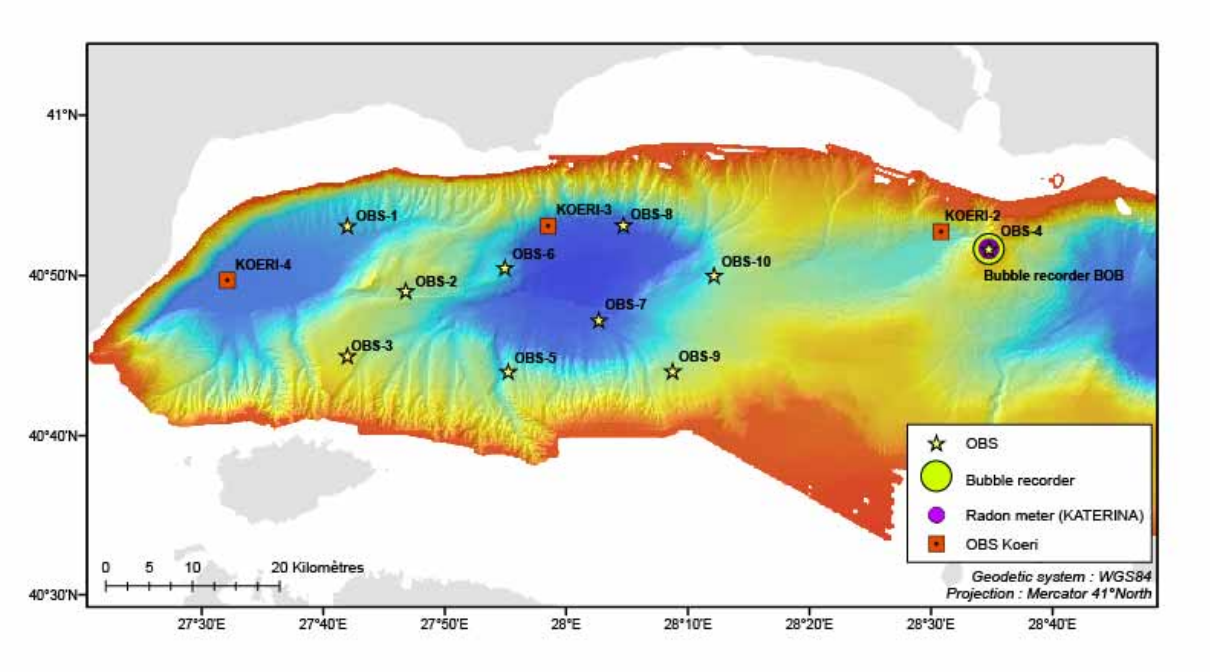

Figure III.1 Bathymetric map of the Western and Central Sea of Marmara. Yellow stars indicate Ifremer OBSs deployed April 15th to July 31st, 2011 (OBS2 failed 31 days before the end of the deployment). Red squares indicate KOERI's permanent submarine stations. The study area is delineated by coordinates 40°43'N - 40°54'N – 27°30'E – 28°15'E (OBS4 and KOERI-2 are not within study area).

III.2 High-resolution velocity model

The objective here is the high-resolution characterization of earthquakes strictly located within the network. Based on previous work *[Tary, 2011; Tary et al., 2011]*, travel times are known to be strongly controlled by the two following factors:

1. the sea bottom topography and the velocity contrast at the water/sediment interface
2. the slow seismic velocities within the sediment infill in the main Marmara Trough.

Consequently, in order to take into account the 2 controlling factors, a velocity model was specifically designed for the study area (see rectangular frame in Figure III.1), considering the geological and seismological knowledge of the Marmara Main Fault acquired since the 1999, Izmit earthquake and all available information, including the seabottom topography derived from the high-resolution (38 m), multibeam bathymetric grid of *[Le Pichon et al, 2001]; and* the pre-kinematic basement topography derived from the tomographic model that was

obtained from the Seismarmara Cruise in 2011, using 650 seismic shots recorded at 37 OBSs [*Bayrakci et al, 2013]*.

We followed the following steps:

1. The initial tomographic model of [*Bayrakci, 2013]* (6 km x 6 km x 2 km) was used as initial model to describe the velocity structure of the pre-kinematic basement down to 12km depth below sea level.
2. The iso-depth contours of the pre-kinematic basement (Top of figure III.2) were used as guide lines to define 9 domains for the study area, having each a "typical" velocity profile down to 12 km depth. These domains have been represented using Matlab (see the files's code : *plotDomain.m*). Each h "typical " profile corresponds to an average curve calculated with Matlab at 5 different depths (0-2-4-6-8 km depth). For instance, for the first domain, the value at 4 km depth corresponds to the mean of values at 4 km for all points constituting the first domain.
3. A dense, high-resolution sub-grid was then defined (using ArcMap) for the study area, with grid spacing 750 m x 750 m x 400 m, by sub-dividing the tomographic grid of Bayrakci et al [2013] (6 km = 8 x 750 m) 0.750 km).
4. Each node M of the dense sub-grid was ascribed: to: i) the water depth inferred from the high resolution bathymetric grid of [*Le Pichon et al., 2001];* ii) to a given domain N (with N=1 to 9, as defined in Figure III.3). The velocity structure at grid node M for the upper 12 km is provided by the characteristic velocity profile of domain N.
5. Below 12 km and down to 36 km, the velocity structure is assumed to depend on longitude and inferred from the Wide-Angle Reflexion results of [*Bécel et al., 2009],* as explained in Figure III.7 and III.8. Velocities of 6.7 km/s and 8 km/s were ascribed to the lower crust and upper mantle respectively.
6. Each point of the fine su-grid is thus characterized by : depth, "domain" number, "typical" velocity profile above 12 km, depth of lower crust, depth of Moho.

Algorithm: (Matlab files's code : *modele36km.m*)

- from 0 km to point's depth : 1,5km/s
- from point's depth to 12 km : linear interpolation between Bayrakci's point every 2 km
- from 12km to lower crust : speed equal to 12 km depth's one
- from lower crust to Moho : speed equal to 6,7 km/s
- from Moho to 36 km depth : speed equal to 8 km/s

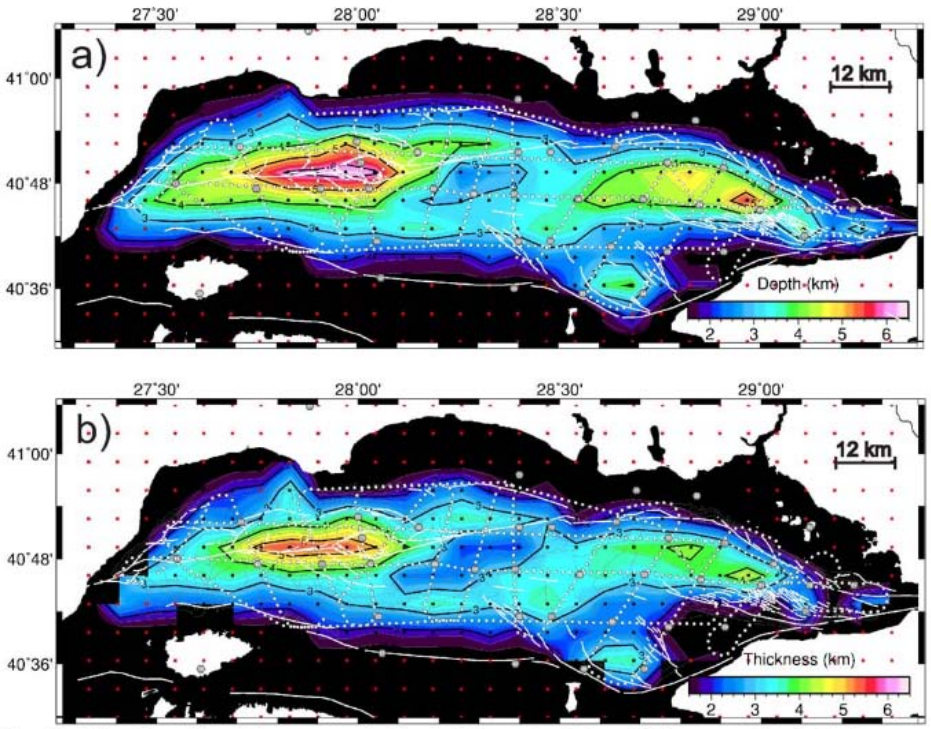

Figure 13. (a) Map of the pre-kinematic basement topography. Submarine fault scarps after Armijo *et al.* 2002 are represented in white. Black crosses are inverted nodes and red ones are fixed ones. Receivers (OBSs and land stations) are represented in grey hexagons. (b) Map of the sedimentary thickness obtained by subtracting the seafloor depth from the basement depth at grid node positions.

Figure III.2. [(after Bayrakci et al, 2013] : Map of pre-kinematic basement topography, based on the seismic tomography experiment carried out during the Seismmarmara Cruise in 2011. White and grey dots are respectively shots and receivers.

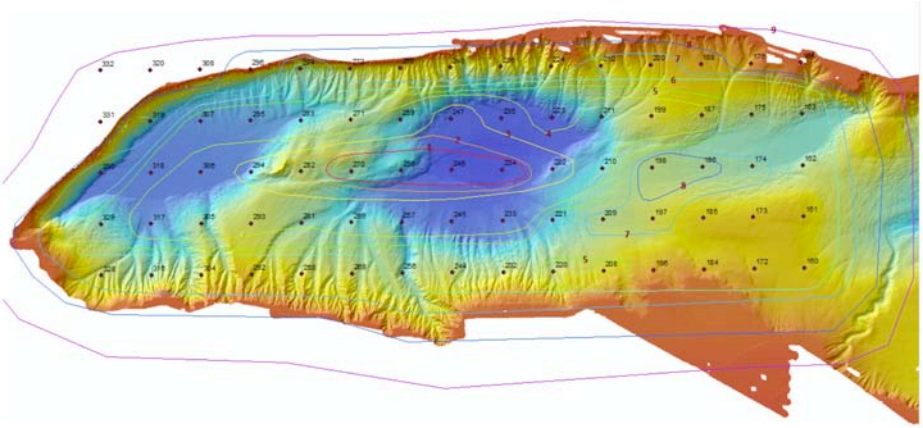

Figure III.3 : Bathymetric map of the western the Sea of Marmara, with dots indicating grid nodes (with 6 km x 6 km spacing) from the tomographic model of Bayrakci et al.,l [2013]. Colour lines are based on iso-depth contours of the pre-kinematic basement inferred from the tomographic model (see top figure in Fig. III.2). These contour lines are used here to delineate 9 domains having a characteristic velocity structure in the upper 12 kilometers (see figures III.4, III.5 and III.6) . Domain 1 is delineated by contour 1. Domain N is between contours N-1 and N (N=2 to 9).

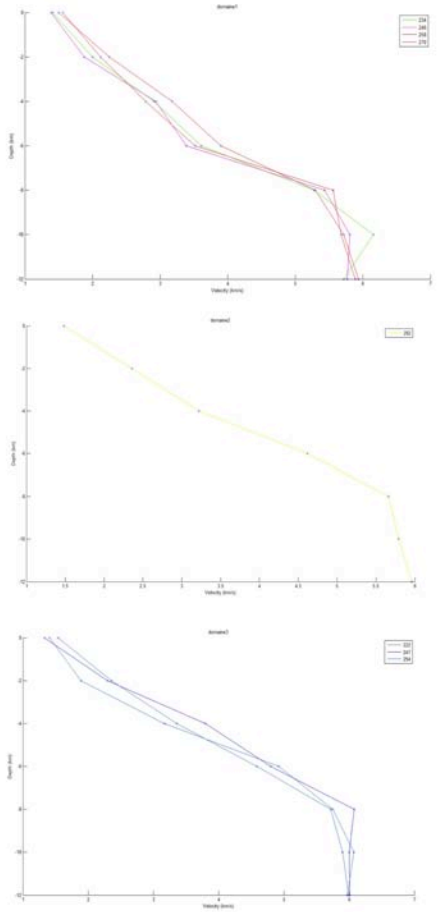

Figure III.4. Velocity profiles within domains 1 (top), 2 (middle) and 3 (bottom).

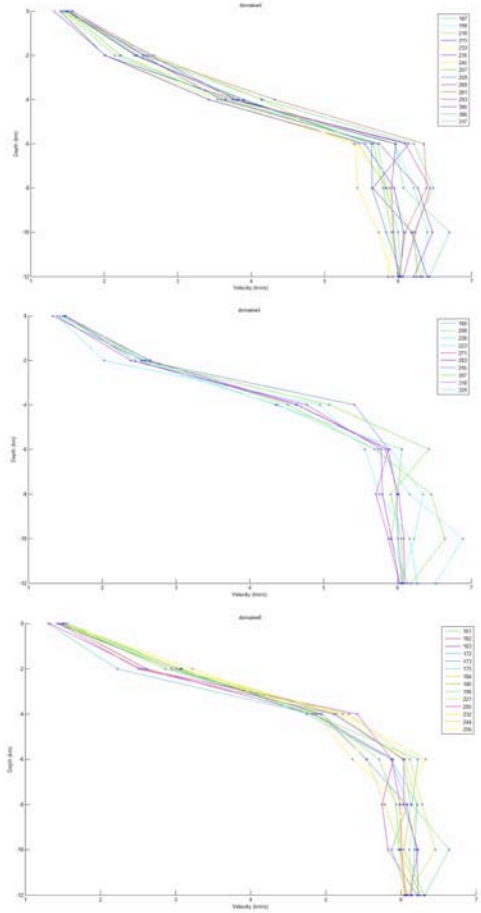

Figure III.5. Velocity profiles within domains 4 (top), 5 (middle) and 6 (bottom).

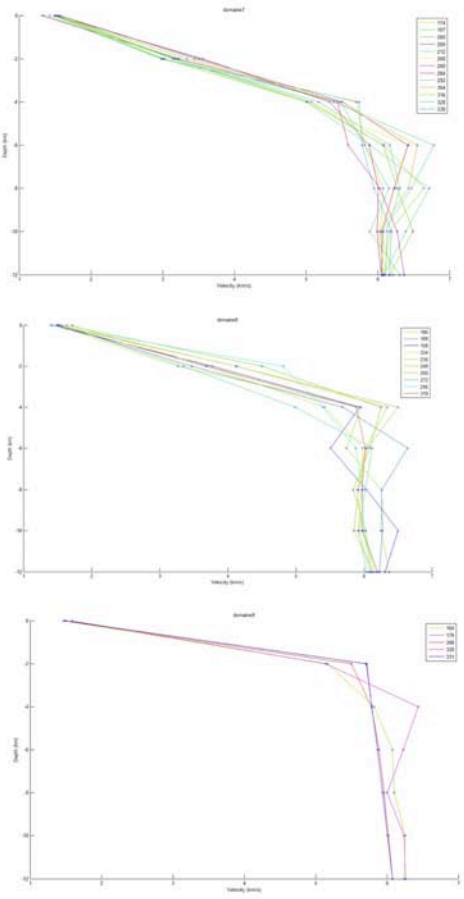

Figure III.6. Velocity profiles within domains 7 (top), 8 (middle) and 9 (bottom).

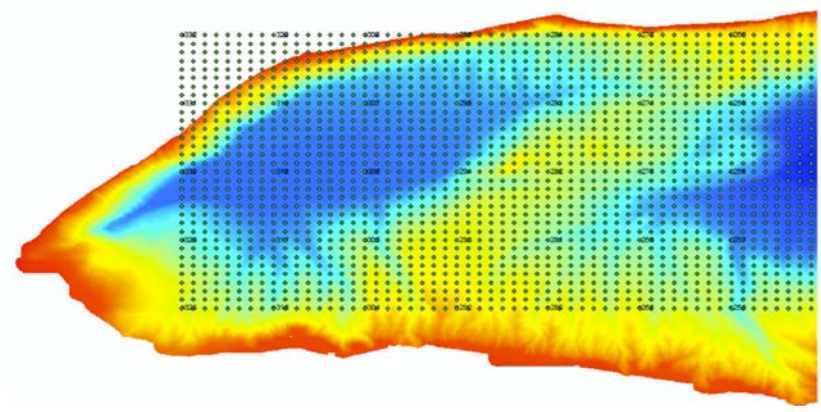

Figure III.7. Final grid nodes (with node spacing of 750 m x 750 x 400 m) used in the present study for the high-resolution characterization of earthquakes in the Western Sea of Marmara. Numbers indicate grid nodes from [Bayrakci et al., 2013]. Each final grid node M is ascribed to: i) the water depth inferred from the high resolution bathymetric grid of [Le Pichon et al., 2001]; ii) to a given domain N (with N=1 to 9, as defined in Figure III.3). The velocity structure at grid node M for the upper 12 km is provided by the characteristic velocity profile of domain N. Below 12 km, the velocity structure is assumed to depend on longitude and inferred from the Wide-Angle Reflexion results of [Bécel et al., 2009], as explained in Figure III.8 and III.9.

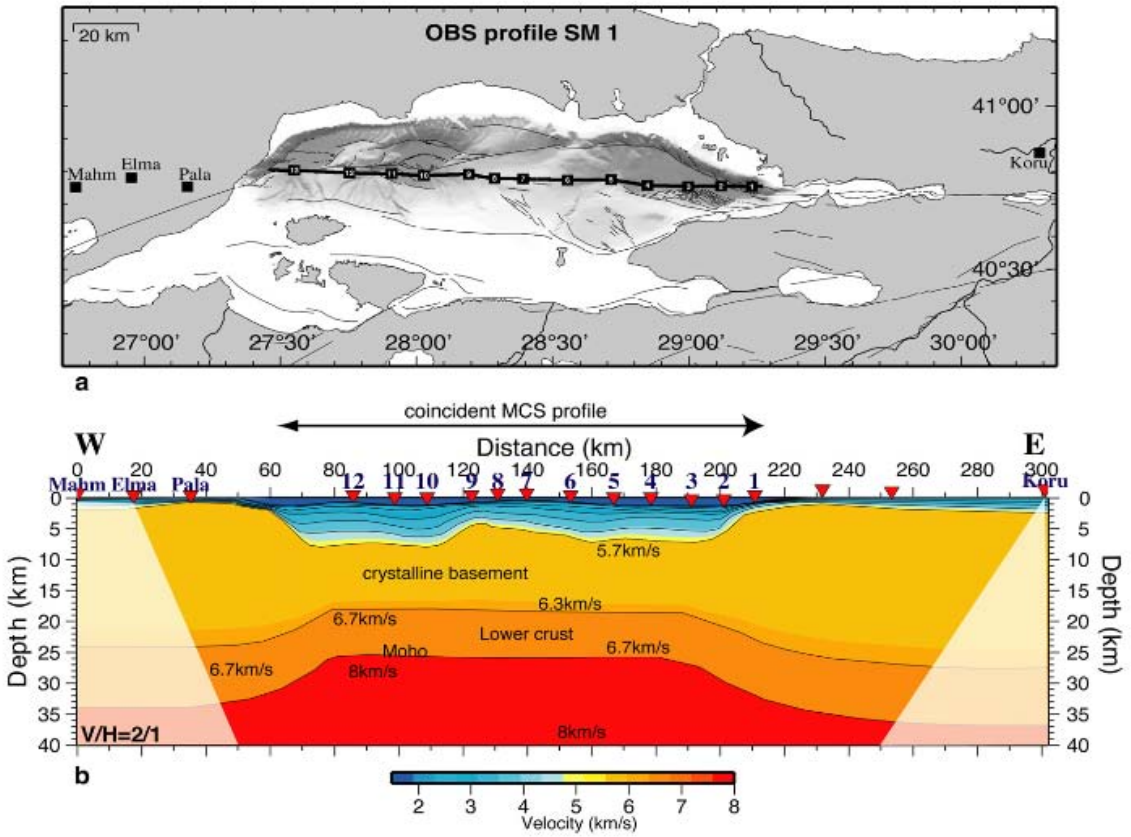

Fig. 3. a) Location map of the EW regional OBS profile SM-1/23 — black squares onshore indicate the land station, black squares offshore the ocean bottom seismometers. b) Final P-waves velocity depth model from wide angle reflection–refraction data (WARR) with color scale at the bottom. Black arrows indicate the coincident multichannel seismic profile SM-1/23. Vertical exaggeration of 2.

Figure III.8 : After [Bécel et al., 2019]. P-wave velocity inferred from wide-anglereflexion seismics along an E-W line running across the Sea of Marmara. The velocity structure for the lower crust and Moho, of each grid node M (see caption, Figure 12) is assumed to depend on longitude.

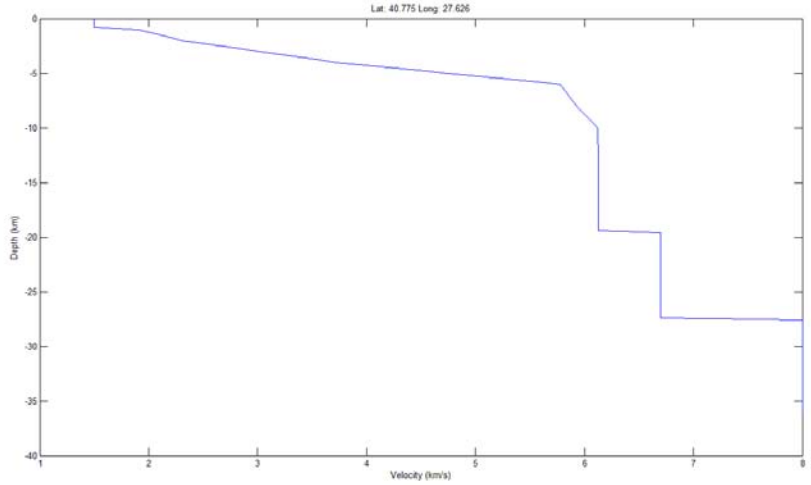

Figure III.9 : Example of final velocity profile at grid point with coordinates 40.775°N, 27.626°E. The velocity profile from 0 to 12 km is inferred from the bathymetric grid of [Le Pichon et al., 2001] and from the tomographic grid of [Bayrakci et al, 2013], as explained in the text and in Figure III.6. From 12 to 25 km, the velocity profile is considered as depending only on longitude and inferred from the Wide-Angle results of [Bécel et al., 2009].

III.3 High-resolution characterization of the aftershock sequence that followed the Mw 5.2 earthquake on July, 25th, 2011

During the recording period, a Mw 5.2 earthquake occured on July, 25th, 2011, at 17h57, followed by a 3-days long sequence of aftershocks. This section strictly focuses on the fine characterization of this sequence (Figure III.9), which was obtained following a two-steps procedure: 1) absolute locations were first obtained using a 3D-velocity model and NLLOC, a non linear routine developed by Lomax [xx]; then, relative locations were obtained using HYPODD *[Waldhauser et al, 2000]* and the 1-D velocity model of *Tary et al. [2011]*.

Locations using the 6 km x 6 km x 2 km 3D-velocity model of Bayrakci et al [2013] (Figs. III.10 to III.12). Absolute locations are evenly distributed between the sea-floor and 15 km at depth, with most of the seismicity concentrated on the Western High (Figure 10 top). Still, many aftershocks are located away from the mainshock and delineate an E-W trend below the Tekirdag Basin. Relative localization using HypoDD strongly reduces the RMS and focuses the seismicity along the fault on top of the Western High. Still, many events are found in the Tekirdag Basin along the same E-W trend (Figure 10 middle). In the vertical section (Figure 10 bottom), relative locations appear distributed into 2 groups of events, between the sea-floor and 6 km depth, and between 6 and 12 km depth, respectively.

In order to eliminate possible artifacts related to the uneven distribution of OBSs, we considered a specific sub-network defined by 4 stations symmetrically distributed on a circle more or less centered on the mainshock : 3 IFREMER OBSs *(OBS1*, *OBS6* and *OBS3)*, and one KOERI station *(KOERI4*). Only those events having arrivals picks on the 4 OBSs were considered. Using the 3D velocity model of Bayrakci et al. [2013], most absolute locations appear to be mostly focused on the Western High and located at a depth above 15 km (Figure 12 top). Relative localization using HypoDD results in improved focusing above the Western High and shallower events (depth < 10 km). Interestingly, two groups of earthquakes appear: one with depths between 0 and 5 km; and one with depths between 8 and 14 km.

Locations using the Bayrakci-Coutellier-Cros 3D-velocity model with grid mesh size of 1500 m x 1500 m x 400 m (BCC-1 model) (Figs. III.13 and III.14). Absolute locations are dispersed within the Tekirdag Basin, with E-W trends (Fig. III.13 top). Relative locations obtained with HypoDD are more focused near the epicenter of the mainshock (Fig. III.13 middle) and shallower (Fig. III.13 bottom) than with the Bayrakci's model.

Absolute and relative locations obtained with the BCC-1 model and picks from the sub-network only, appear to be much more focused and closer from the fault (Figure III.14 top and middle) than those obtained with the Bayrakci et al. [2013] model (Figure III.12 top and middle). Interestingly, two different groups of events clearly appear: one with relative location depths between 0 and 5 km; and one with relative location depths between 8 and 14 km (Fig. III.14).

Location using the Bayrakci-Coutellier-Cros 3D-velocity model with grid mesh size of 750 m x 750 m x 200 m (BCC-2 model) (Fig. III.15 and III.16). The general trends described above (with BCC-1 model) are enhanced when using the BBC-2 model. Absolute locations are dispersed within the Tekirdag Basin, with E-W trends (Fig. III.15 top). Relative locations obtained with HypoDD are more focused near the epicenter of the mainshock (Fig. III.15 middle) and shallower (Fig. III.15 bottom) than with the Bayrakci's or the BCC-1 model.

Both absolute and relative locations obtained with the BCC-2 model and picks from the sub-network only, appear to be much more focused and closer from the fault (Figure III.16 top and middle) than those obtained with the Bayrakci et al. [2013] and BCC-1 models (respectively Fig. III.12 and III.14, top and middle). Again, two different groups of events clearly appear: one with relative location depths between 0 and 5 km; and one with relative location depths between 8 and 14 km (Fig. III.16 bottom to be compared with Fig. III.14 bottom and Fig. III.12 bottom).

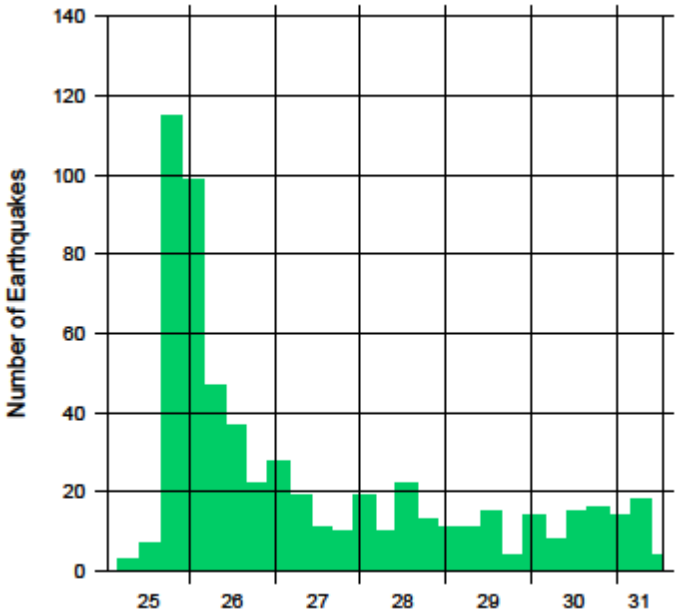

Figure III.9: Histogram showing the number of events (over 6 hours periods) detected by the different OBSs, following the Mw 5.2 earthquake that occurred on July 25th, 2011, at 17:57. Almost half of the aftershocks occurred within the first 12 hours after the mainshock.

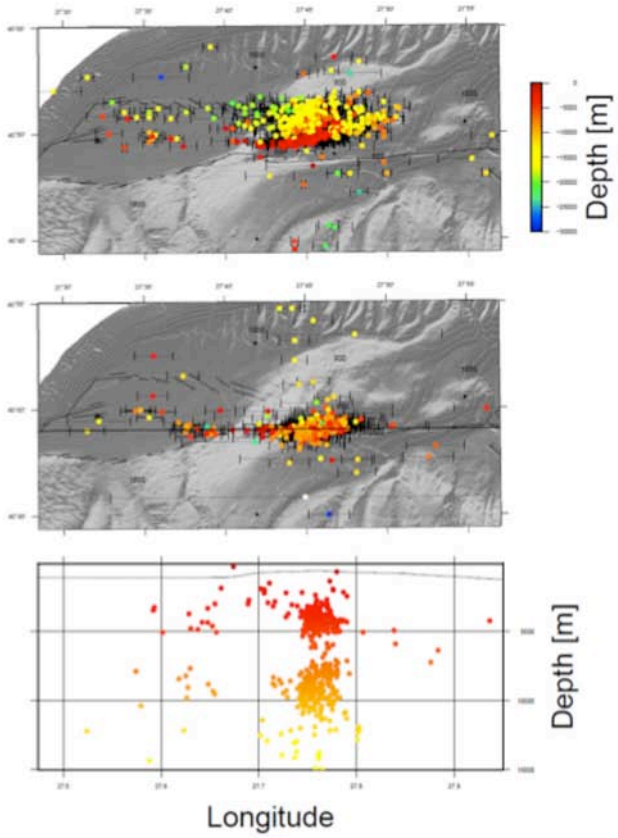

Fig. III.10 Top : Absolute locations of aftershocks using the 3D velocity model of Bayrakci et al. [2013] and NLLOC developed by Anthony Lomax. Middle : relative locations using the 1D velocity model of Tary et al. [2011] and hypoDD [Waldhauser et al, 2000]. Bottom : Vertical cross-section showing depth distribution of epicenters (relative locations).

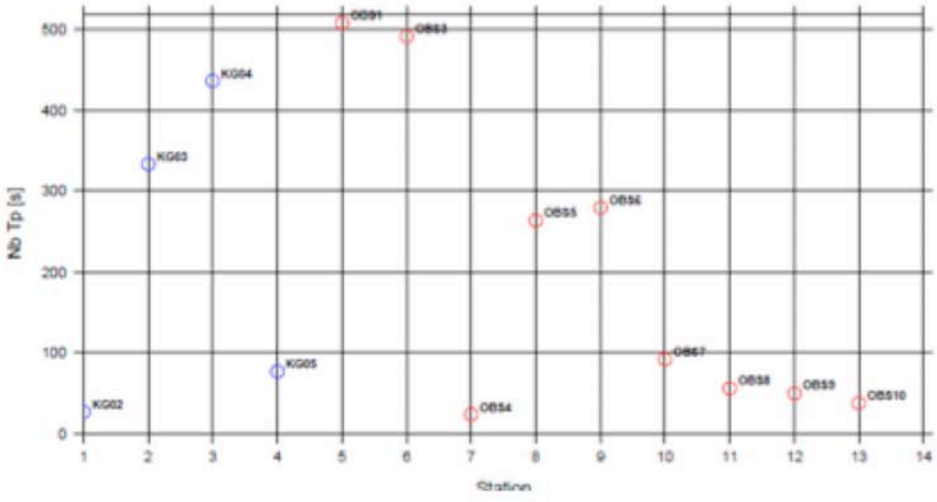

Fig. III.11 Number of picks detected at each OBS (IFREMER and KOERI)

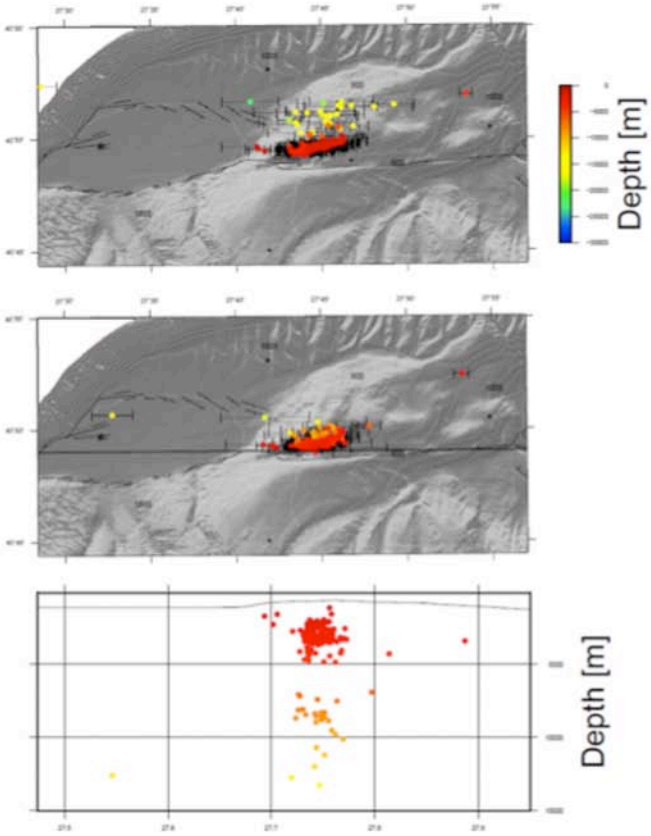

Fig. III.12 In order to eliminate possible artifacts related to the uneven distribution of OBSs, we considered a specific sub-network defined by 4 stations symmetrically distributed on a circle more or less centered on the mainshock : 3 IFREMER OBSs (OBS1, OBS6 and OBS3), and one KOERI station (KOERI4). Only those events having arrivals picks on the 4 OBSs are here considered in the present figure. Top : Absolute locations of aftershocks using the 3D velocity model of Bayrakci et al. [2013] and NLLOC developed by Anthony Lomax. Middle : relative locations using the 1D velocity model of Tary et al. [2011] and hypoDD [Waldhauser et al, 2000]. Bottom : Vertical cross-section showing depth distribution of epicenters (relative locations).

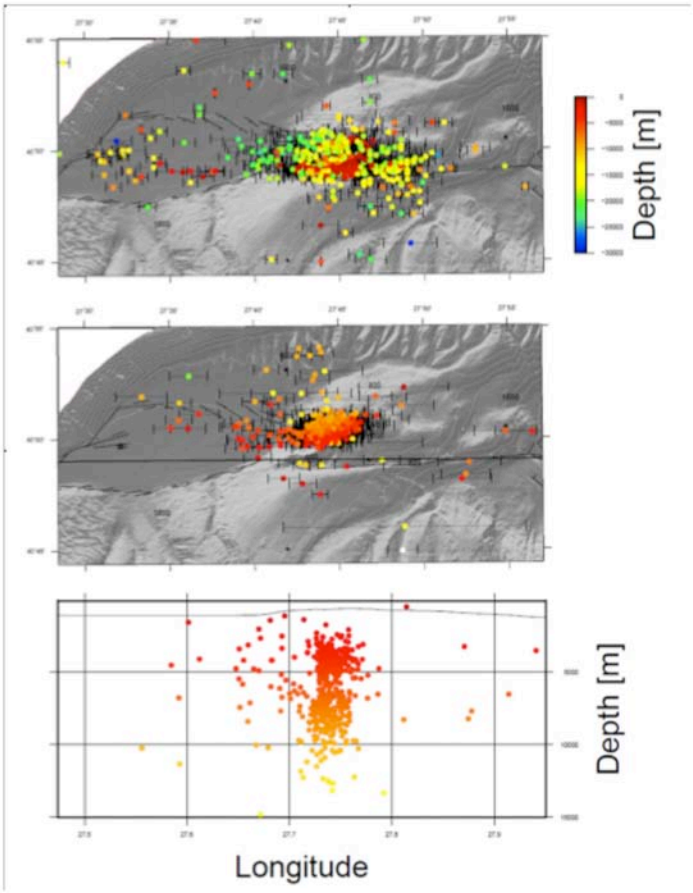

Fig. III.13 Top : Absolute locations of aftershocks using the BCC-1, 3D velocity model (1.5 km x 1.5 km x 0.4 km) and NLLOC developed by Anthony Lomax. Middle : relative locations using the 1D velocity model of Tary et al. [2011] and hypoDD [Waldhauser et al, 2000]. Bottom : Vertical cross-section showing depth distribution of epicenters (relative locations).

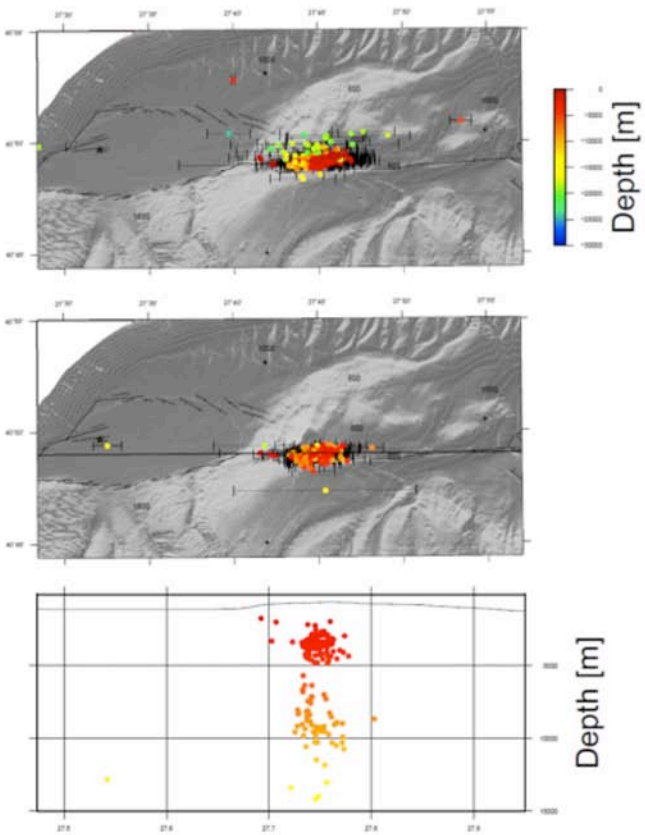

Fig. III.14 In order to eliminate possible artifacts related to the uneven distribution of OBSs, we considered a specific sub-network defined by 4 stations symmetrically distributed on a circle more or less centered on the mainshock : 3 IFREMER OBSs (OBS1, OBS6 and OBS3), and one KOERI station (KOERI4). Only those events having arrivals picks on the 4 OBSs are here considered in the present figure. Top : Absolute locations of aftershocks using the BCC-1, 3D velocity model (1.5 km x 1.5 km x 0.4 km) and NLLOC developed by Anthony Lomax. Middle : relative locations using the 1D velocity model of Tary et al. [2011] and hypoDD [Waldhauser et al, 2000]. Bottom : Vertical cross-section showing depth distribution of epicenters (relative locations).

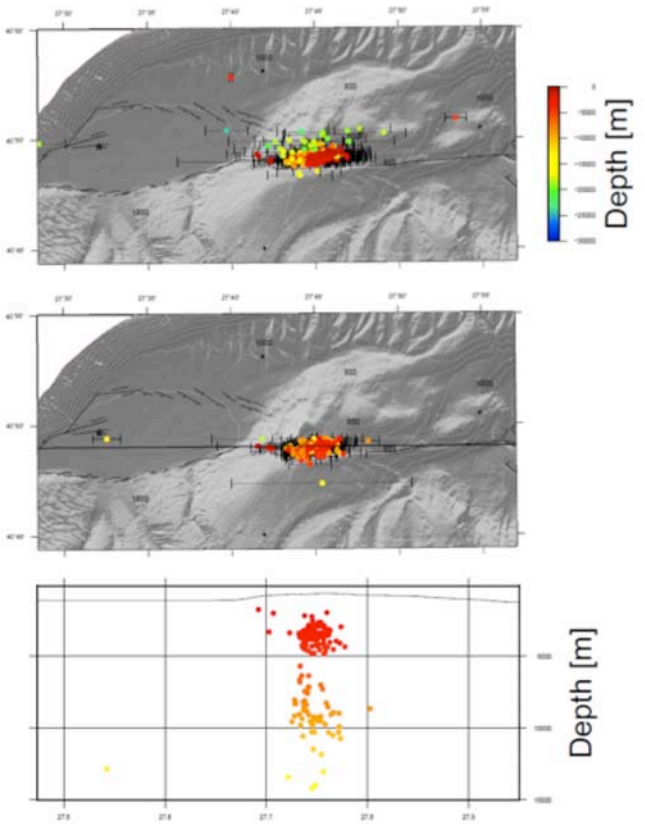

Fig. III.14 In order to eliminate possible artifacts related to the uneven distribution of OBSs, we considered a specific sub-network defined by 4 stations symmetrically distributed on a circle more or less centered on the mainshock : 3 IFREMER OBSs (OBS1, OBS6 and OBS3), and one KOERI station (KOERI4). Only those events having arrivals picks on the 4 OBSs are here considered in the present figure. Top : Absolute locations of aftershocks using the BCC-1, 3D velocity model (1.5 km x 1.5 km x 0.4 km) and NLLOC developed by Anthony Lomax. Middle : relative locations using the 1D velocity model of Tary et al. [2011] and hypoDD [Waldhauser et al, 2000]. Bottom : Vertical cross-section showing depth distribution of epicenters (relative locations).

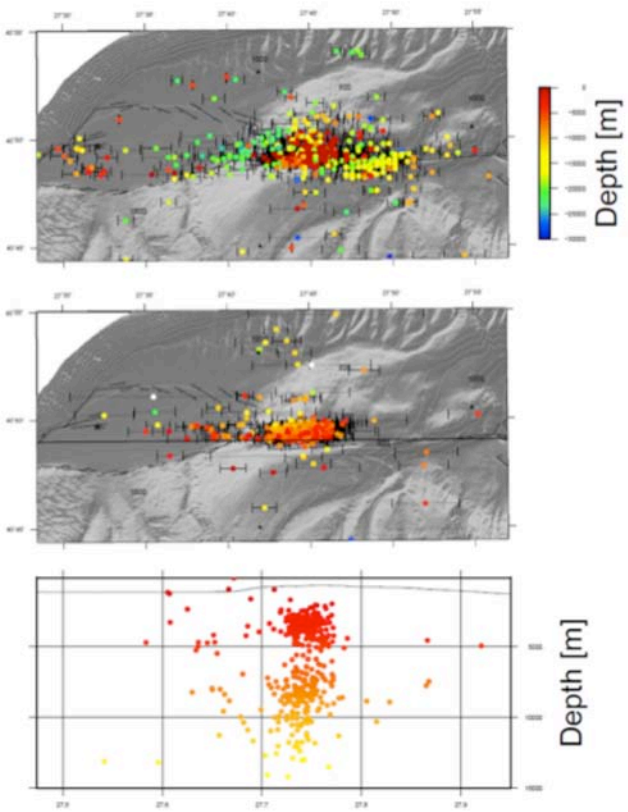

Fig. III.15 Top : Absolute locations of aftershocks using the BCC-2, 3D velocity model (750 m x 750 m x 200 m) and NLLOC developed by Anthony Lomax. Middle : relative locations using the 1D velocity model of Tary et al. [2011] and hypoDD [Waldhauser et al, 2000]. Bottom : Vertical cross-section showing depth distribution of epicenters (relative locations).

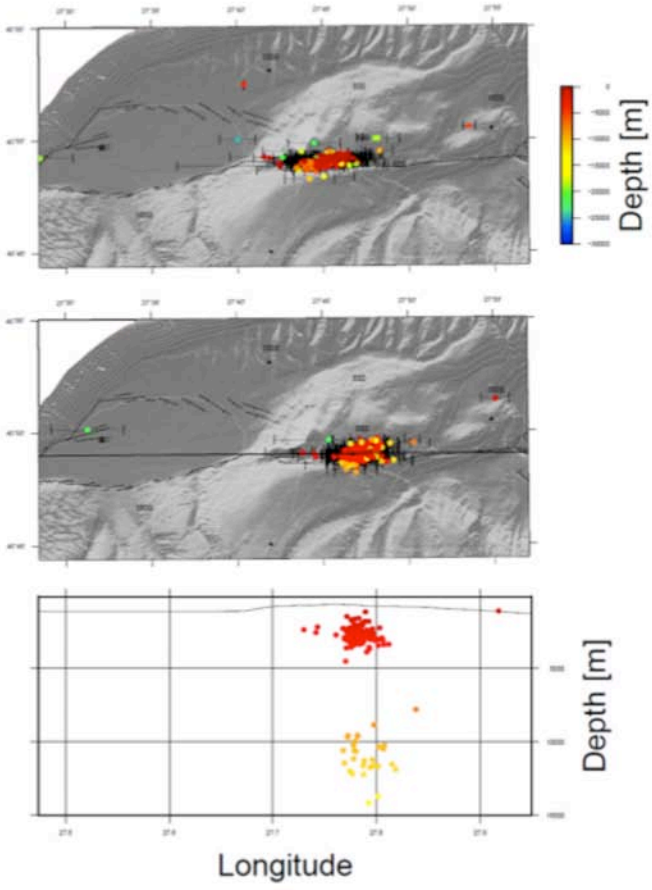

Fig. III.16 In order to eliminate possible artifacts related to the uneven distribution of OBSs, we considered a specific sub-network defined by 4 stations symmetrically distributed on a circle more or less centered on the mainshock : 3 IFREMER OBSs (OBS1, OBS6 and OBS3), and one KOERI station (KOERI4). Only those events having arrivals picks on the 4 OBSs are here considered in the present figure. Top : Absolute locations of aftershocks using the BCC-2, 3D velocity model (750 m x 750 m x 200 m) and NLLOC developed by Anthony Lomax. Middle : relative locations using the 1D velocity model of Tary et al. [2011] and hypoDD [Waldhauser et al, 2000]. Bottom : Vertical cross-section showing depth distribution of epicenters (relative locations).

IV. Conclusion

Because the basins of the Sea of Marmara are filled with more than 5 km of Plio-Quaternary soft ("slow") sediments, the velocity structure of the offshore domain is drastically different from the one onshore. Therefore, merging land and sea-bottom datasets is a very difficult challenge.

- The velocity model developed by KOERI for the whole Marmara region by merging land and sea stations will be very useful to improve the quality of earthquake catalogs and the real time monitoring of the régional seismicity.
- In contrast, to improve the final-scale location of hypocenters near the submerged fault zone and enhance the search for seismic tremors [*Bouchon et al.,* 2011], specific networks of permanent, cabled sea-bottom seismometers are required. Each network should be consistent *per se*, and allow the high-resolution characterization of earthquakes below the Sea of Marmara. In addition, it is of critical importance to create an high-resolution, 3D velocity model, in order to take into account for the velocity contrast at the water/sediment interface and the slow seismic velocities within the sediment infill in the main Marmara Trough.
- In the present report, a high-resolution, 3D velocity model was built for a 20 km x 60 km area located in the Western Sea of Marmara (750 m x 750 m x 430 m grid spacing). The seabottom topography was derived from a high-resolution grid (38 m) based on mulitbeam bathymetric data collected in 2000 *[Le Pichon et al., 2001]*. *Th*e structure of the sediment basin was determined using: i) the 3D tomographic model of *[Bayracki et al., 2013]*; ii) velocity models along 2D, wide-angle seismics lines *[Bécel et al., 2010*]; iii) all the geological information from the Marmara Sea resulting from the numerous cruises that have been carried out the Sea of Marmara since 1999.
- Comparable, high-resolution velocity models are still needed for the Central and Eastern parts of the Marmara Trough.

REFERENCES

Bécel, A. (2006). *Structure sismique de la Faille Nord Anatolienne en Mer de Marmara*, Université Denis Diderot.

Bécel, A.; Laigle, M.; de Voogd, B.; Hirn, A.; Taymaz, T.; Galvé, A.; Shimamura, H.; Murai, Y.; Lépine, J.-C.; Sapin, M. & Özalaybey, S. (2009). Moho, crustal architecture and deep deformation under the North Marmara Trough, from the SEISMARMARA Leg 1 offshore-onshore reflection-refraction survey, *Tectonophysics* **467**: 1-21.

Bécel, A.; Laigle, M.; de Voogd, B.; Hirn, A.; Taymaz, T.; Yolsal-Cevikbilen, S. & Shimamura, H. (2010). North Marmara Trough architecture of basin infill, basement and faults, from PSDM reflection and OBS refraction seismics, *Tectonophysics* **490** : 1-14.

Bayrakci, G.; Laigle, M.; Bécel, A.; Hirn, A.; Taymaz, T.; Yolsal-Cevikbilen, S. & team, S. (2013). *3-D sediment-basement tomography of the Northern Marmara trough by a dense OBS network at the nodes of a grid of controlled source profiles along the North Anatolian fault*, *Geophys. J. Int*. **194** : 1335-1357

Bohnhoff, M.; Bulut, F.; Dresen, G.; Malin, P. E.; Eken, T. & Aktar, M. (2013). *An earthquake gap south of Istanbul*, *Nat Commun*. **4** : -.

Bouchon, M. Karabulut, H., Aktar, M., Ozalabey, S., Schmittbuhl, Bouin, M.-P., (2011), Extended Nucleation of the 1999 *M*w 7.6 Izmit Earthquake, *Science*, **331**, 877, doi:10.1126/science.1197341

Bourry, C., Chazallon, B., Charlou, J-L, Donval J.P, Ruffine, L., Henry, P., Geli, L., Çagatay, M.N., Sedat, İ, Moreau, M., (2009). Free gas and gas hydrates from the Sea of Marmara, Turkey: Chemical and structural characterization. *Chem. Geol.,* doi:10.1016/j.chemgeo.2009.03.007

Gürbüz, C.; Aktar, M.; Eyidogan, H.; Cisternas, A.; Haessler, H.; Barka, A.; Ergin, M.; Türkelli, N.; Polat, O.; Üçer, S.; Kuleli, S.; Baris, S.; Kaypak, B.; Bekler, T.; Zor, E.; Bicmen, F. & Yoruk, A. (2000). The seismotectonics of the Marmara region (Turkey): results from a microseismic experiment, *Tectonophysics* **316** : 1-17.

Géli, L.; Henry, P.; Zitter, T.; Dupré, S.; Tryon, M.; Cagatay, M.; de Lépinay, B. M.; Le Pichon, X.; Sengor, A.; Gorur, N.; Natalin, B.; Ucarkus, G.; Ozeren, S.; Volker, D.; Gasperini, L.; Burnard, P.; Bourlange, S. & the Marnaut Scientific Party (2008). Gas emissions and active tectonics within the submerged section of the North Anatolian Fault zone in the Sea of Marmara, *Earth Plan. Sci. Lett.* **274** : 34-39.

Hergert, T.; Heidbach, O.; Bécel, A. & Laigle, M. (2011). *Geomechanical model of the Marmara Sea regionaI. 3-D contemporary kinematics*, Geophysical Journal International 185 : 1073-1089.

Hubert-Ferrari, A.; Barka, A.; Jacques, E.; Nalbant, S. S.; Meyer, B.; Armijo, R.; Tapponnier, P. & King, G. C. P. (2000). Seismic hazard in the Marmara Sea region following the 17 August 1999 Izmit earthquake, *Nature* **404** : 269-273.

Karabulut, H.; Schmittbuhl, J.; Özalaybey, S.; Lengliné, O.; Kömeç-Mutlu, A.; Durand, V.; Bouchon, M.; Daniel, G. & Bouin, M. (2011*). Evolution of the seismicity in the eastern Marmara Sea a decade before and after the 17 August 1999 Izmit earthquake*, *Tectonophysics* **510** : 17-27.

Laigle, M.; Becel, A.; de Voogd, B.; Hirn, A.; Taymaz, T. & Ozalaybey, S. (2008). *A first deep seismic survey in the Sea of Marmara: Deep basins and whole crust architecture and evolution*, Earth and Planetary Science Letters 270 : 168-179.

Le Pichon, X.; Sengor, A.; Demirbag, E.; Rangin, C.; Imren, C.; Armijo, R.; Gorur, N.; Cagatay, N.; Mercier de Lepinay, B.; Meyer, B.; Saatcilar, R. & Tok, B. (2001). *The active Main Marmara Fault*, *Earth Plan. Sci. Lett*., **192** : 595-616.

Lomax, A., C. Satriano and M. Vassallo (2012), Automatic picker developments and optimization: FilterPicker - a robust, broadband picker for real-time seismic monitoring and earthquake early-warning, Seism. Res. Lett. , **83**, 531-540, doi: 10.1785/gssrl.83.3.531.

Lomax, A. and A. Michelini (2012), Tsunami early warning within 5 minutes, *Pure and Applied Geophysics*, **169**, doi: 10.1007/s00024-012-0512-6.

Lomax, A., A. Michelini, A. Curtis (2009), Earthquake Location, Direct, Global-Search Methods, in *Complexity In Encyclopedia of Complexity and System Science, Part 5, Springer, New York*, pp. 2449-2473, doi:10.1007/978-0-387-30440-3.

Lomax, A., J. Virieux, P. Volant and C. Berge, (2000), Probabilistic earthquake location in 3D and layered models: Introduction of a Metropolis-Gibbs method and comparison with linear locations, in *Advances in Seismic Event Location, Thurber, C.H., and N. Rabinowitz (eds.), Kluwer*, Amsterdam, 101-134

Meade, B. J.; Hager, B. H.; McClusky, S. C.; Reilinger, R. E.; Ergintav, S.; Lenk, O.; Barka, A. & Özener, H. (2002). *Estimates of Seismic Potential in the Marmara Sea Region from Block Models of Secular Deformation Constrained by Global Positioning System Measurements*, *Bull. Seism. Soc. Am.*, **92** : 208-215.

Meghraoui, M.; Aksoy, M. E.; Akyuz, H. S.; Ferry, M.; Dikbas, A. & Altunel, E. (2012). Paleoseismology of the North Anatolian Fault at Güzelköy (Ganos segment, Turkey): Size and recurrence time of earthquake ruptures west of the Sea of Marmara, *Geochemistry, Geophysics, Geosystems* **13**.

Orgülü, G. (2011). *Seismicity and source parameters for small-scale earthquakes along the splays of the North Anatolian Fault (NAF) in the Marmara Sea*, Geophysical Journal International 184 : 385-404.

Stewart, S. W., 1981. *Principles and applications of microearthquake networks*. Academic Press, .

Tary, J. B.; Géli, L.; Henry, P.; Natalin, B.; Gasperini, L.; Comoglu, M.; Cagatay, N. & Bardainne, T. (2011). Sea-Bottom Observations from the Western Escarpment of the Sea of Marmara, *Bull. Seism. Soc. Am.*, **101** : 775-791.

Tryon, M. D.; Henry, P. & Hilton, D. R. (2012). Quantifying submarine fluid seep activity along the North Anatolian Fault Zone in the Sea of Marmara, *Marine Geology* 315-318 : 15-28.

Waldhauser, F. & Ellsworth, W. L. (2000). A Double-Difference Earthquake Location Algorithm: Method and Application to the Northern Hayward Fault, California, *Bull. Seism. Soc. Am.*, **90** : 1353-1368.